Water Resources Research

RESEARCH ARTICLE
10.1029/2023WR035056

Can a Sparse Network of Cosmic Ray Neutron Sensors Improve Soil Moisture and Evapotranspiration Estimation at the Larger Catchment Scale?

Fang Li[1,2,3], Heye Reemt Bogena[1], Bagher Bayat[1], Wolfgang Kurtz[1,2,4], and Harrie-Jan Hendricks Franssen[1,2]

[1]Agrosphere Institute, Forschungszentrum Jülich GmbH, Jülich, Germany, [2]Centre for High-Performance Scientific Computing in Terrestrial Systems: HPSC TerrSys, Geoverbund ABC/J, Jülich, Germany, [3]Faculty of Georesources and Materials Engineering, RWTH Aachen University, Aachen, Germany, [4]Department of Agrometeorology, Now at Deutscher Wetterdienst, Freising, Germany

Key Points:

- Assimilation of soil moisture from a network of cosmic-ray neutron sensors improves soil moisture characterization at the catchment scale
- Soil moisture characterization improved more in a wet year than in a very dry year
- Evapotranspiration and river discharge simulation are only slightly improved, despite better estimations of soil moisture

Correspondence to:
F. Li,
f.li@fz-juelich.de

Citation:
Li, F., Bogena, H. R., Bayat, B., Kurtz, W., & Hendricks Franssen, H.-J. (2024). Can a sparse network of cosmic ray neutron sensors improve soil moisture and evapotranspiration estimation at the larger catchment scale? *Water Resources Research*, *60*, e2023WR035056. https://doi.org/10.1029/2023WR035056

Received 6 APR 2023
Accepted 28 NOV 2023

Author Contributions:
Data curation: Fang Li, Wolfgang Kurtz
Formal analysis: Fang Li, Heye Reemt Bogena, Bagher Bayat, Harrie-Jan Hendricks Franssen
Funding acquisition: Fang Li
Supervision: Harrie-Jan Hendricks Franssen
Validation: Fang Li
Visualization: Fang Li
Writing – original draft: Fang Li
Writing – review & editing: Fang Li, Heye Reemt Bogena, Bagher Bayat, Harrie-Jan Hendricks Franssen

Abstract Cosmic-ray neutron sensors (CRNS) fill the gap between locally measured in-situ soil moisture (SM) and remotely sensed SM by providing accurate SM estimation at the field scale. This is promising for improving hydrologic model predictions, as CRNS can provide valuable information on SM in the root zone at the typical scale of a model grid cell. In this study, SM measurements from a network of 12 CRNS in the Rur catchment (Germany) were assimilated into the Terrestrial System Modeling Platform (TSMP) to investigate its potential for improving SM, evapotranspiration (ET) and river discharge characterization and estimating soil hydraulic parameters at the larger catchment scale. The data assimilation (DA) experiments (with and without parameter estimation) were conducted in both a wet year (2016) and a dry year (2018) with the ensemble Kalman filter (EnKF), and later verified with an independent year (2017) without DA. The results show that SM characterization was significantly improved at measurement locations (with up to 60% root mean square error (RMSE) reduction), and that joint state-parameter estimation improved SM simulation more than state estimation alone (more than 15% additional RMSE reduction). Jackknife experiments showed that SM at verification locations had lower and different improvements in the wet and dry years (an RMSE reduction of 40% in 2016 and 16% in 2018). In addition, SM assimilation was found to improve ET characterization to a much lesser extent, with a 15% RMSE reduction of monthly ET in the wet year and 9% in the dry year.

1. Introduction

Soil moisture has a significant influence on water and energy fluxes between the subsurface, land surface, and the atmosphere (Chen & Hu, 2004). Accurate information on the spatio-temporal variability of soil moisture is crucial to better understand the role of soil moisture in terrestrial systems (Vereecken et al., 2022). Soil moisture can be estimated at various scales, indirectly with remote sensing (RS) observations and directly by in situ measurements using electromagnetic techniques being the most commonly used methods. The resolution of RS-derived products is often coarse, spatially or temporally, and the data are subjected to various errors, especially in areas with dense vegetation coverage (Bauer-Marschallinger et al., 2019; Kim et al., 2020). On the other hand, in situ measurements are point-scale measurements and, therefore, do not provide area coverage (He et al., 2021).

Over the last decade, the CRNS has been introduced as an alternative method, providing real-time soil moisture estimation and bridging the gap between in-situ measurements and RS products. The CRNS footprint covers up to 18 ha with a measurement depth of up to 80 cm (Bogena et al., 2015; Köhli et al., 2015; Zreda et al., 2008). The continuous development of CRNS technology has enabled SM monitoring under a variety of climatic conditions, which has promoted its application in hydrological modeling (R. Baatz et al., 2017), satellite product validation (Zhao et al., 2021), extreme weather event (drought and flood risk) assessment (Bogena et al., 2022), ecohydrological (e.g., snow, precipitation, and vegetation) monitoring (Bogena et al., 2020), and agricultural management (Li et al., 2019). The advantages of CRNS have made it increasingly attractive, and large-scale CRNS networks have been established in Europe, the USA, Australia, and India for large-scale soil moisture monitoring with high temporal resolution, which can also benefit the multifaceted hydrological applications mentioned above.

However, it is neither economical nor feasible to measure area-wide soil moisture over large areas using CRNS. Therefore, it is important to establish a scientific and economical observation network that can cover all major

land use types and climatic zones in the study area while ensuring that the sensor coverage is representative of soil moisture patterns across the region. Then hydrological or land surface models can be combined with observations to effectively monitor soil moisture at larger scales, including unobserved locations, and validate the model's performance.

Nevertheless, modeling accuracy is often limited by uncertainties arising mainly from model forcings, parameters, and initial conditions (R. Baatz et al., 2017; Freeze, 1975). Data assimilation (DA) is a technique to combine different information sources to update or correct the model predictions and improve the simulations (De Lannoy et al., 2014). The Ensemble Kalman filter (Evensen, 1994, 2003), a sequential filtering algorithm, is the most widely used DA technique and has been proven effective for nonlinear systems and high-dimensional problems (Camporese et al., 2009; Schöniger et al., 2012). The process of DA can be summarized in two steps: a forecast step and an analysis step. For the forecast step, the state estimation is only based on past data, while for the analysis step, the probability density of the state is propagated forward, considering the information from current measurements (McLaughlin, 2002).

Shuttleworth et al. (2013) developed the forward COsmic-ray Soil Moisture Interaction Code (COSMIC) model to enable rapid conversion of neutron counts to soil moisture values. Since then, COSMIC has been used as an observation operator in several studies for assimilating neutron counts into land surface models to improve soil moisture prediction (R. Baatz et al., 2017; Han et al., 2015, 2016; Patil et al., 2021; Rosolem et al., 2014; Shuttleworth et al., 2013). For example, R. Baatz et al. (2017) found that catchment-scale soil moisture prediction can be improved by assimilating soil moisture from a CRNS network and that joint estimation of state and parameters performs better than state estimation alone. To date, however, such assimilation experiments with CRNS data have been conducted only with land surface models that do not adequately describe lateral water movement and groundwater-land surface interactions (Kollet & Maxwell, 2008). Zhao et al. (2021) compared the CRNS data with simulated soil moisture using both the land surface model Community Land Model (CLM, version 3.5) and a coupled land surface-subsurface model (CLM-ParFlow). They found that the coupled model simulations showed less bias and reproduced better soil moisture dynamics than the CLM stand-alone, demonstrating the importance of considering lateral subsurface flow in subsurface hydrological simulations. Therefore, there is still strong interest in applying DA with coupled land surface-subsurface models to exploit the full potential of CRNS data.

In this work, the integrated Terrestrial System Modeling Platform (Kurtz et al., 2016; Shrestha et al., 2014) is used, which is a coupled atmosphere-land surface-subsurface model with the Parallel Data Assimilation Framework (PDAF). The integrated model TSMP has been utilized in a number of studies (Furusho-Percot et al., 2019; Keune et al., 2016; Shrestha et al., 2015; Shrestha, Sulis, et al., 2018). Previous studies investigating the assimilation of soil moisture measurements with TSMP-PDAF focused on synthetic experiments, small catchments, or greatly simplified the representation of spatial heterogeneity in the real catchment (Gebler et al., 2019; Hung et al., 2022; Zhang et al., 2018). Recently, Hung et al. (2022) adopted the conventional vertical weighting calculation of CRNS data from Franz et al. (2012) for the assimilation of soil moisture data in a virtual reality experiment with TSMP and discovered that DA improved the vertical soil moisture profile characterization and soil moisture estimation for the surrounding grid cells.

In this study, soil moisture from a distributed network of 12 CRNS in the Rur catchment was assimilated into TSMP to investigate whether the sensor density is sufficient to represent the SM for the whole catchment. So far, to the best of our knowledge, this is the first study to assimilate soil moisture from such a high-density CRNS monitoring network into the integrated model. Our work, for the first time, explores the information content of CRNS observations through fully coupled TSMP and data assimilation techniques. It unlocks the full potential of CRNS to characterize the SM and ET across a relatively large catchment. The main objectives of this study are to investigate: (a) how effective a CRNS network can be in improving soil moisture characterization with fully integrated terrestrial models such as TSMP at the catchment scale; (b) whether the assimilation of CRNS soil moisture data can result in better prediction of ET and discharge; and (c) how DA performance can vary between years with different hydrological conditions (wet vs. dry).

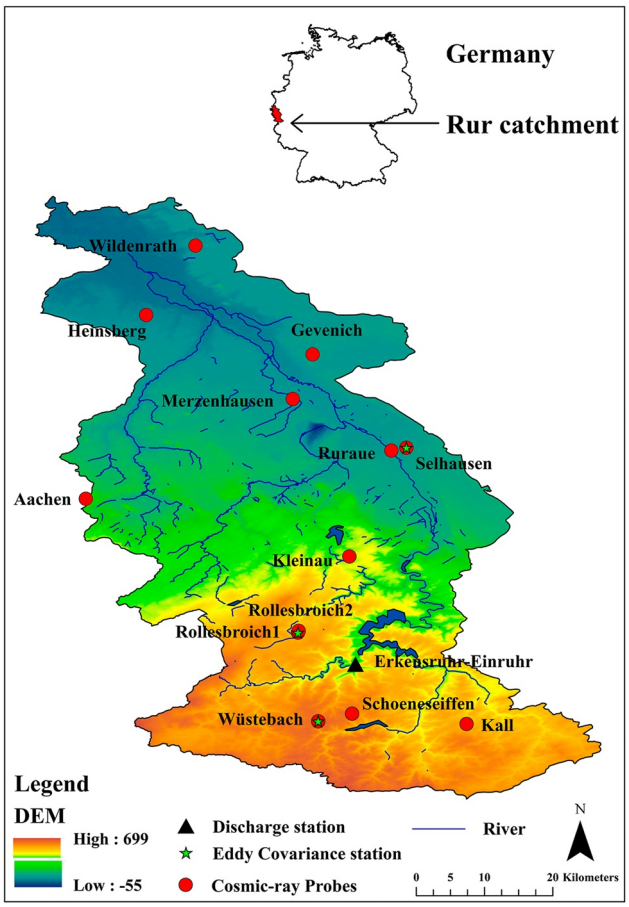

Figure 1. Map of the Rur catchment with the altitude above sea level and the locations of the cosmic-ray neutron sensors, eddy covariance stations and discharge station. The Rur catchment is situated in western Germany.

2. Materials and Methods

2.1. Study Area

The Rur catchment covers an area of 2,354 km^2 and is located in western Germany, including small portions of Belgium and the Netherlands. Figure 1 shows the Digital Elevation Model (DEM) for the Rur catchment obtained from SRTM 90m Version 4 (Jarvis et al., 2008). The Rur River flows from the Eifel low-mountain range in the south with a maximum altitude of 690 m a.s.l. to the northern lowlands with a minimum altitude of 15 m a.s.l. The land use types in the Rur catchment are arable agriculture in the north (mainly maize and wheat) and grassland, coniferous and deciduous forests in the south (R. Baatz et al., 2017; Waldhoff & Lussem, 2015). From the northern to the southern part of the catchment, long-term average annual precipitation ranges from 650 to 1,300 mm, the mean annual air temperature decreases from 10 to 7°C, and the mean annual potential evapotranspiration ranges from 450 to 850 mm (Bogena et al., 2018; Montzka et al., 2008). The mean river discharge in the upper catchment (controlled by the in situ station Erkensruhr-Einruhr (see Figure 1)) was about 0.26 m^3/s from 2013 to 2022.

2.2. Terrestrial System Modeling Platform (TSMP)

TSMP is a modular coupled biogeophysical terrestrial systems model consisting of atmospheric, surface, and subsurface models (Shrestha et al., 2014). The three component models that make up TSMP are the numerical weather prediction model COSMO (Consortium for Small Scale Modeling) (Baldauf et al., 2011), the Community Land Model CLM3.5 (Oleson et al., 2004, 2008) from the National Center for Atmospheric Research, and the 3D variably saturated groundwater flow model ParFlow (Kollet & Maxwell, 2006) for the subsurface. These three models are two-way coupled by the Ocean Atmosphere Sea Ice Soil coupling Model Coupling Toolkit (OASIS-MCT, version 3) (Valcke, 2013). The OASIS-MCT coupler is included in the model platform and is used for the exchange of variables and fluxes between different sub-models. In this work, only the land surface model CLM3.5 and the subsurface model ParFlow were used.

The biophysical processes simulated by the land surface model CLM3.5 include energy and water exchange between the land and atmosphere, snow accumulation and melting, energy and water transport in the soil, and stomatal physiology and photosynthesis (Oleson et al., 2004, 2008). Spatial land surface heterogeneity is represented by the nested subgrid hierarchy in CLM (Oleson et al., 2008). Each grid cell is divided into different types of land units (glacier, lake, wetland, urban, and vegetated), and each land unit in the grid cell can have a different number of snow/soil columns, and each column can have multiple plant functional types (PFTs) with different plant physiological parameters (Bonan et al., 2002; Oleson et al., 2008), for example, leaf area index (LAI). The input LAI used in this study was taken from previous studies, in which the study area included the Rur domain (Sulis et al., 2015, 2018). The primary function of the CLM in the TSMP is to calculate evapotranspiration from the ground and vegetation. See Appendix A for details on the computing of evapotranspiration by CLM.

In the coupled model TSMP, the hydrological processes of the CLM are replaced by ParFlow (Ashby & Falgout, 1996; Jones & Woodward, 2001; Kollet & Maxwell, 2006; Maxwell, 2013). ParFlow solves the 3D Richards equation (Richards, 1931) for groundwater flow in the unsaturated and saturated zones and the kinematic wave equation (Lighthill & Whitham, 1955) for overland flow. The coupled partial differential equations for subsurface flow and surface water flow are solved by the Newton-Krylov nonlinear solver (Jones & Woodward, 2001). Moreover, ParFlow was created for parallel computing systems and can effectively solve large-scale problems at high resolution, which has been proven in numerous studies (Hung et al., 2022; Jones & Woodward, 2001; Kollet & Maxwell, 2006, 2008). In addition, ParFlow employs a terrain-following grid

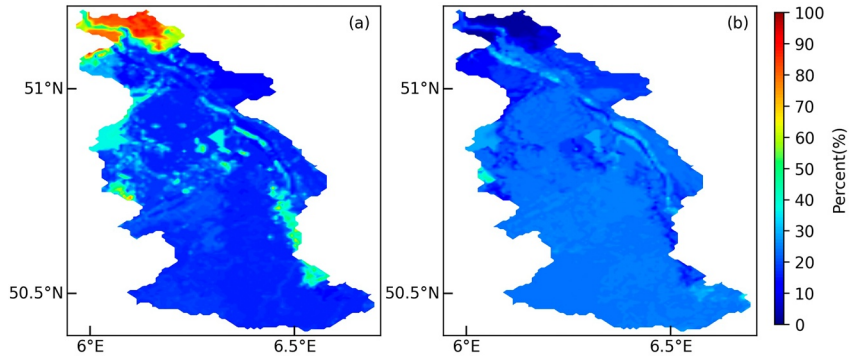

Figure 2. Sand (a) and clay content (b) for the Rur catchment derived from the BK50 soil map.

transformation with variable vertical discretization, which can resolve groundwater problems with high topographic gradients and reduce the computation time (Maxwell, 2013).

The coupler OASIS-MCT controls the exchange of fluxes and state variables between CLM and ParFlow, ensuring that the spatial and temporal scales of the fluxes exchanged by the different components remain consistent (Shrestha et al., 2014; Valcke, 2013). In the coupled model TSMP, ParFlow provides the pressure and saturation of the upper 10 subsurface layers to CLM, while in turn, CLM provides the upper boundary conditions, that is, net infiltration or exfiltration, to ParFlow. The net infiltration includes precipitation, interception, total evaporation, and total transpiration (Zhang et al., 2018). More comprehensive information about the implementation of the coupler in TSMP and its operation is presented by Kurtz et al. (2016).

2.3. Data

2.3.1. Atmospheric Forcing

The high-resolution atmospheric reanalysis data set COSMO-REA6 (0.055° (6 km)) is used as forcing data for the land surface model CLM (Bollmeyer et al., 2015; Wahl et al., 2017). The reanalysis data set was developed by the German Meteorological Service (Deutscher Wetterdienst; DWD) based on the numerical weather prediction (NWP) model COSMO (Baldauf et al., 2011), covering the period 1995–2020, and is continuously being extended. Forcing data include precipitation, air temperature, air pressure, wind velocity, specific humidity, incoming shortwave radiation, and incoming longwave radiation. In addition, to maintain consistency with the atmospheric forcings, daily air pressure and air humidity from COSMO-REA6 were used to calculate the weighting of soil moisture based on the revised approach from Schrön et al. (2017). The coupled model CLM-ParFlow of the Rur domain has a horizontal spatial resolution of 500 m for the land surface and a total depth of 100 m for the subsurface.

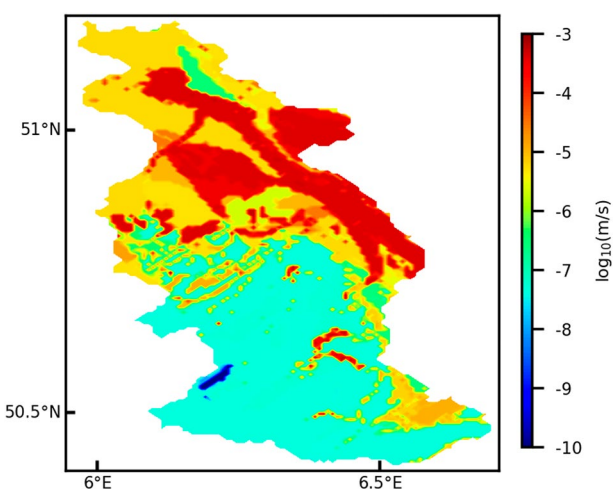

Figure 3. Hydraulic conductivity of the bedrock for the Rur catchment.

2.3.2. Soil Data

The high-resolution regional soil map BK50 (Geologischer Dienst Nordrhein-Westfalen, 2009) at a scale of 1:50,000 (https://www.opengeodata.nrw.de/produkte/geologie/boden/BK/ISBK50/; last access: 7 July 2023) and the European Soil Database (ESDB) (Pano, 2006) were utilized to obtain the soil texture and compute its hydrological parameters. Sand and clay contents (see Figure 2) were derived from BK50, and bulk density was obtained from ESDB.

The aquifer permeability for the layers below the soil layers was taken from the 100 m resolution regional hydraulic conductivity (K_s) map (Figure 3) from the North Rhine-Westphalia Geological Survey database.

2.3.3. CRNS and Flux Data

The CRNS detects epithermal neutrons produced by cosmic radiation, which can be used to measure soil moisture because the detected neutron count rate

Table 1
CRNS Sites Used in This Study, Including Key Site Characteristics

Name	Latitude (°C)	Longitude (°C)	Altitude (m)	Mean annual precipitation (mm y^{-1})	Mean air temperature (°C)	Landuse
Merzenhausen	50.930	6.297	91	718	10.3	Crop
Rollesbroich1	50.622	6.304	515	1,018	7	Grassland
Rollesbroich2	50.624	6.305	506	1,018	7	Grassland
Gevenich	50.989	6.324	107	718	10.3	Crop
Ruraue	50.862	6.427	100	718	10.3	Grassland
Wildenrath	51.133	6.169	72	722	10.3	Needleleaf
Wüstebach	50.505	6.331	605	1,401	7	Spruce
Heinsberg	51.041	6.104	58	722	10.3	Crop
Kall	50.501	6.526	505	857	8	Grassland
Selhausen	50.866	6.447	101	718	10.3	Crop
Schönseiffen	50.515	6.376	611	870	7	Grassland
Kleinhau	50.722	6.372	374	614	9	Grassland
Aachen	50.799	6.025	232	865	10.3	Crop

is inversely correlated with the amount of hydrogen in the soil (Zreda et al., 2008). The CRNS soil moisture data were obtained from the "Data set of COSMOS-Europe: A European network of Cosmic-Ray Neutron Soil Moisture Sensors" (Bogena et al., 2022). The raw neutron count data were measured by the CRNS stations and then transformed into soil moisture values with harmonized correction and processing by Bogena et al. (2022). There are 13 CRNS stations (Andreasen et al., 2017; R. Baatz et al., 2017; Bogena et al., 2022) relatively evenly distributed over the domain (Figure 1), and detailed information is presented in Table 1 for all sites. In this work, the soil moisture measured by CRNS is used for DA and as independent verification data for jackknife simulations. The CRNS stations Rollesbroich1 and Rollesbroich2 are regarded as one site since they are too close and located in the same model grid cell, and the average values for the two sites were used in this study. This is, therefore, equivalent to having 12 CRNS sites for final assimilation.

The observed flux data of three eddy covariance (EC) stations (Rollesbroich, Wüstebach, and Selhausen) and discharge data of the Erkensruhr-Einruhr in situ station from TERENO (TERrestrial ENvironmental Observatories; https://www.tereno.net/; last access: 7 July 2023) were used to verify the evapotranspiration and discharge simulations. The runoff station in the upstream catchment was chosen for validation because the downstream catchment is highly influenced by water management activities (e.g., water reservoirs, wastewater treatment plant discharges, opencast lignite mining) (Bogena et al., 2005). EC measurements have been taken with a sonic anemometer (CSAT3, Campbell Scientific Inc., Logan, USA) to measure the 3D wind components, an open-path gas analyzer (Li7500, LI-COR Inc., Lincoln, USA) to determine the H_2O and CO_2 concentrations in the air, and an air temperature and humidity sensor (HMP45C, Vaisala Inc., Helsinki, Finland). Conversions to fluxes, including uncertainty information, are based on Mauder et al. (2013). The daily EC data were gap-filled by grass reference evapotranspiration calculated from the FAO Penman-Monteith equation (Allan et al., 1998). The non-closure of the energy balance of the EC data was not corrected. For further information on EC measurements and processing, the reader is referred to Bogena et al. (2018).

2.4. Data Assimilation Methodology

The EnKF was used in this work to assimilate soil moisture measured by CRNS into the coupled model TSMP. The EnKF sequentially alternates model prediction and filter updating steps (also called filter analysis), either state updates alone or joint state-parameter updates. The effectiveness of the filter depends on the accurate determination of the forecast error covariance from the ensemble, and the sources of forecast errors are mainly uncertain initial conditions, forcing data, and model equations (Turner et al., 2008). To ensure that errors from various sources are taken into consideration to improve assimilation results, perturbation is used to create an ensemble that takes into account the different error sources. In this work, the ensemble of model realizations takes

into account the uncertainty of model forcings (including precipitation, incoming shortwave radiation, incoming longwave radiation, and air temperature), parameters (including saturated hydraulic conductivity and porosity), and initial conditions (from spin-up).

For each ensemble member i at time step t, the soil moisture state vector $\mathbf{x}_{i,t}$ is updated by the model prediction. The forecast step is given by:

$$\mathbf{x}_{t,i} = f(\mathbf{x}_{t-1,i}, \mathbf{q}_{t,i}, \mathbf{p}_{t,i}) \tag{1}$$

where i is the ensemble member, $\mathbf{x}_{t,\,i}$ is the model forecast state vector at time step t, f is the model TSMP, $\mathbf{x}_{t-1,\,i}$ is the earlier model analysis state vector at time step $t-1$, $\mathbf{q}_{t,\,i}$ is the vector with (perturbed) model forcings and $\mathbf{p}_{t,\,i}$ denotes the model perturbation vector with parameters. Model forecasts are updated according to:

$$\mathbf{x}_{t,i}^{a} = \mathbf{x}_{t,i}^{f} + \mathbf{K}_t\left(\mathbf{y}_{t,i} - \mathbf{H}_t\mathbf{x}_{t,i}^{f}\right) \tag{2}$$

where $\mathbf{y}_{t,\,i}$ is the vector with (perturbed) observations, and the superscripts a and f refer to the updated state vector (the analysis) and the model predicted state vector, respectively. The observation operator $\mathbf{H}_t$ is used to map model forecasts into the observation space, which is assumed to be linear, and $\mathbf{K}_t$ denotes the Kalman gain that is calculated as:

$$\mathbf{K}_t = \mathbf{P}_t\mathbf{H}_t^T\left(\mathbf{H}_t\mathbf{P}_t\mathbf{H}_t^T + \mathbf{R}_t\right)^{-1} \tag{3}$$

where $\mathbf{P}_t$ is the model covariance matrix, which is calculated from the forecasted ensemble of model simulations at time step t according to:

$$\mathbf{P}_t = \frac{\sum_{i=1}^{N}\left(\mathbf{x}_{t,i}^{f} - \overline{\mathbf{x}}^{f}\right)\left(\mathbf{x}_{t,i}^{f} - \overline{\mathbf{x}}^{f}\right)^T}{N-1} \tag{4}$$

where $\overline{\mathbf{x}}^{f}$ is a vector with ensemble mean values for the model states at time step t. $\mathbf{R}_t$ is the measurement error covariance matrix, which is defined based on the expected measurement error of the CRNS soil moisture data (0.03 cm^3/cm^3). N is the number of ensemble members.

The updated states are then finally given by:

$$\mathbf{x}_{t,i}^{a} = \mathbf{x}_{t,i}^{f} + \mathbf{P}_t\mathbf{H}_t^T\left(\mathbf{H}_t\mathbf{P}_t\mathbf{H}_t^T + \mathbf{R}_t\right)^{-1}\left(\mathbf{y}_{t,i} - \mathbf{H}_t\mathbf{x}_{t,i}^{f}\right) \tag{5}$$

In this work, the EnKF is also used to update the most sensitive parameter (saturated hydraulic conductivities) in ParFlow. The other parameters were not updated because Brandhorst & Neuweiler, 2023 found that updating multiple parameters for the unsaturated zone is prone to causing numerical instabilities, even in synthetic studies. The augmented state vector for updating both states and parameters is then extended and defined as follows:

$$\mathbf{x}_{t,i}^{f} = \begin{pmatrix} \boldsymbol{\psi}_{t,i} \\ \mathbf{Y}_{t,i} \end{pmatrix} \tag{6}$$

where $\mathbf{x}$ is the augmented state vector, including pressure heads ($\boldsymbol{\psi}$) (m) and the logarithm of hydraulic conductivities ($\mathbf{Y} = \log_{10}K_s$ (m/s)).

A damping factor ($\boldsymbol{\alpha}$) is used when both states and parameters are updated, so as to reduce filter inbreeding (Hendricks Franssen & Kinzelbach, 2008; Hung et al., 2022). Filter inbreeding refers to the underestimation of the ensemble variance that occurs after the EnKF analysis is applied repeatedly, which happens when the ensemble size is small (Hendricks Franssen & Kinzelbach, 2008). The damping factor could reduce the modification of the forecast with the Kalman gain and limit the intensity of the perturbation of the parameter ($\log_{10}K_s$) (Gebler et al., 2019). This results in the following updating equation for the joint state-parameter estimation:

$$\mathbf{x}_{t,i}^{a} = \mathbf{x}_{t,i}^{f} + \alpha^T\mathbf{P}_t\mathbf{H}_t^T\left(\mathbf{H}_t\mathbf{P}_t\mathbf{H}_t^T + \mathbf{R}_t\right)^{-1}\left(\mathbf{y}_{t,i} - \mathbf{H}_t\mathbf{x}_{t,i}^{f}\right) \tag{7}$$

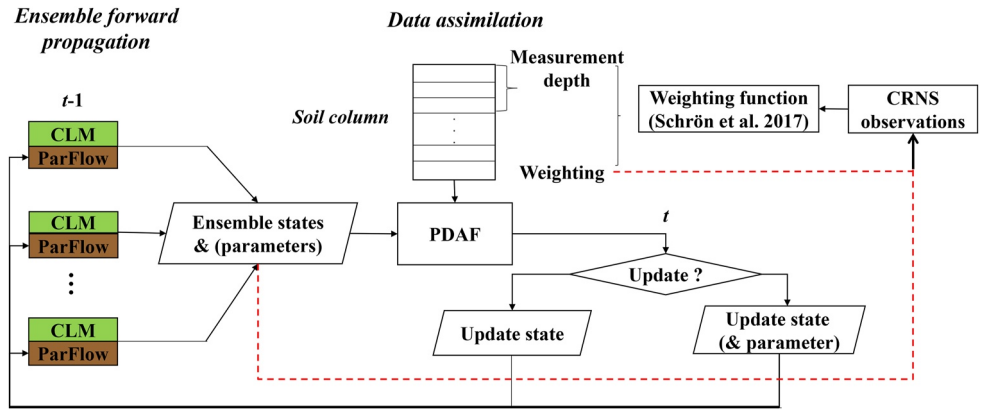

Figure 4. Schematic overview of the assimilation of soil water content from CRNS with PDAF into TSMP (CLM-ParFlow). The flows represented by the red dashed line are outside TSMP-PDAF, including the weighting calculation and the comparison of CRNS soil moisture with the simulations.

where $\boldsymbol{\alpha}^{T}$ is a vector with damping factors, of which 1 is for updating states and values between 0 and 1 are for updating parameters.

The data assimilation updates states (and possibly also parameters) at all grid cells via the calculated model covariances, which give the covariances between all grid cells. Thus, during the analysis step, the states or parameters of the unassimilated locations are also updated, and the update is influenced by the correlation with the states or parameters of the assimilated locations.

3. Model and Experiment Setup

3.1. TSMP-PDAF Setup

The operation mode of TSMP-PDAF, when applied with the assimilation of CRNS soil moisture, is schematically illustrated in Figure 4. Before assimilation, the measurement depth needs to be determined. In order to determine a reasonable penetration depth for the CRNS observations for the corresponding model grid (500m), a mean value for three distances to the CRNS station (2, 25, and 85 m) was calculated based on the revised method of Schrön et al. (2017). This calculation is necessary because the penetration depth depends on the distance to the CRNS station. And then the CRNS soil moisture observation is specified by PDAF for the soil layers until the measurement depth.

The states and parameters of each TSMP realization run are collected by PDAF after a predefined assimilation interval (Gebler et al., 2019). By assimilating soil moisture observations, either model states or both model states and parameters are updated and passed back to the TSMP realizations, and then the updated states and parameters are used in the next prediction step, which is subsequently used in the next analysis, and so on. After the update has been made, the average weighted soil moisture from the simulations is compared with the observed soil moisture from CRNS.

We took the soil layers above 80 cm into account when calculating the weights to be assigned to the different soil layers for their contribution to the CRNS measurement signal. We calculated the weights for 1 mm thick soil layers and integrated the values to calculate the normalized weights for each model soil layer. Readers are referred to Schrön et al. (2017) for a more detailed description of weighting calculations.

3.2. Ensemble Generation

The soil moisture DA experiments employ the EnKF with a total of 128 ensemble members. Each ensemble member was perturbed, with perturbations for meteorological forcings (precipitation, incoming shortwave radiation, longwave radiation, and air temperature), hydraulic conductivity, and porosity to account for uncertainties. The perturbed values were drawn from a multivariate normal distribution, considering the temporal correlation of the four meteorological variables, which were induced by a first-order autoregressive model (Han et al., 2015;

Table 2
The Listed Cross-Correlations Give the Cross-Correlations Between the Perturbations for the Different Atmospheric Variables, Following the Order as Indicated in the Left Column of the Table

Variables	Noise	Standard deviation	Time correlation scale	Cross correlation
Precipitation	Multiplicative	0.3	24 hr	[1.0, −0.8, 0.5, 0.0
Shortwave radiation	Multiplicative	0.2	24 hr	−0.8, 1.0, −0.5, 0.4
Longwave radiation	Additive	20 W m^{-2}	24 hr	0.5, −0.5, 1.0, 0.4,
Air temperature	Additive	1 K	24 hr	0.0, 0.4, 0.4, 1.0]

Reichle et al., 2010). Table 2 summarizes the atmospheric forcing perturbations. The temporal correlations and standard deviations of the perturbations were assigned on the basis of earlier catchment-scale and regional-scale DA studies (R. Baatz et al., 2017; Han et al., 2013, 2015; Reichle et al., 2010). To ensure mass and energy balance, the perturbed precipitation and shortwave radiation are multiplied by the corrected lognormally distributed noises (Han et al., 2013; Yamamoto, 2007).

The vertical profile of the model has a vertical extension of 100 m and is discretized into 25 layers with varying thicknesses. The upper 10 layers extend to 3 m, which coincides with the CLM soil layers, and the lower layers are treated as bedrock layers. The K_s and porosity of the soil and bedrock layers were perturbed separately.

For the soil layers, soil texture (sand and clay contents) was perturbed by geostatistical simulation. A spherical variogram model was adopted to generate a spatially correlated random field with zero mean, variance $50\%^2$ and correlation length of 12.5 km, and the generated perturbation field was added to the original soil texture as derived from the soil map. The sand and clay contents were perturbed separately. The percentages for sand and clay were limited to a range between 0% and 100% to prevent unphysical values for soil texture. The final silt contents were calculated from the perturbed sand and clay contents. Subsequently, the Rosetta pedotransfer functions (Schaap et al., 2001; Zhang & Schaap, 2017) were employed to calculate the perturbed K_s and porosity based on the perturbed soil texture.

For the bedrock layers, the original K_s values are from the hydrogeological map (Figure 3). For each ensemble member, the $\log_{10}K_s$ of all the bedrock layers were perturbed by additive random values (same values for each ensemble member) from a univariate uniform distribution with values between −0.5 and 0.5. The porosity for the lower bedrock layers was set to a constant value of 0.15.

3.3. Setup of the DA Experiments

After generating the ensemble, spin-up simulations for the ensemble members were performed in order to achieve a dynamic groundwater equilibrium. The multi-year average water table depth derived by Bogena et al. (2005) was used as the initial condition, and the 30-year average recharge values (derived from gridded German Meteorological Service data on precipitation and actual evapotranspiration) were used as the upper boundary condition for the ParFlow model. The spin-up simulations for ParFlow were conducted for 100 years. Next, the final conditions from ParFlow's spin-up were used to continue the spin-up for TSMP, including both CLM and ParFlow. This was done for a period of 5 years, using atmospheric forcings from the year 2015 (for the DA experiments in the wet year 2016) or the year 2017 (for the DA experiments in the dry year 2018) as input.

The CRNS soil moisture data were assimilated into the model TSMP by PDAF. In the DA experiments, the states were updated daily by DA, and saturated hydraulic conductivity was updated every 3 days. Those are the optimal updating frequencies found after conducting different assimilation experiments. When jointly updating states and parameters, a damping factor of 0.1 was employed to limit the intensity of the hydraulic conductivity perturbation (Hung et al., 2022) and reduce the possibility of filter inbreeding (Hendricks Franssen & Kinzelbach, 2008). The river grid cells were masked during assimilation analysis to avoid instabilities. The year 2017 is used as an independent evaluation period for the DA experiments of 2016 and 2018. For the year 2017, the ensemble model ran with the updated parameters from 2016 to 2018, but without assimilation.

In addition to the DA experiments, jackknife simulations were also carried out to assess the effect of the CRNS assimilation on soil moisture simulation at unassimilated locations in the model domain. When performing a

Table 3
List of Conducted Simulation Experiments: Open Loop (OL), Data Assimilation With State Update (State) or Joint State and Parameter Update (Joint), Jackknife Evaluation Runs (Jackknife), and Verification Experiments in 2017 Using the Updated Saturated Hydraulic Conductivity (K_s) From Joint Assimilation Experiments of 2016 and 2018 (Updated K_s From 2016 and Updated K_s From 2018)

Year	Experiment	Update state	Update parameter
2016	OL	−	−
	State	+	−
	Joint	+	+
	Jackknife	+	+
2018	OL	−	−
	State	+	−
	Joint	+	+
	Jackknife	+	+
2017	OL	−	−
	Updated K_s from 2016	−	−
	Updated K_s from 2018	−	−

jackknife simulation, 11 sites were used for assimilation (jointly updating states and parameters with a damping factor of 0.1), and the remaining one site was used for evaluation, so there were 12 jackknife experiments for each assimilation year (2016 and 2018). Table 3 lists all the experiments conducted.

3.4. Evaluation of Model Performance

The simulated soil moisture results were evaluated with the following statistical metrics: bias (BIAS), mean absolute error (MAE), correlation coefficient (R), RMSE, and unbiased root mean square difference (ubRMSD):

$$\mathrm{BIAS} = \sum_{t=1}^{n}\left(\mathrm{SM}_t^{\mathrm{sim}} - \mathrm{SM}_t^{\mathrm{obs}}\right) \tag{8}$$

$$\mathrm{MAE} = \frac{\sum_{t=1}^{n}\left(\left|\mathrm{SM}_t^{\mathrm{sim}} - \mathrm{SM}_t^{\mathrm{obs}}\right|\right)}{n} \tag{9}$$

$$R = \frac{\sum_{t=1}^{n}\left(\mathrm{SM}_t^{\mathrm{obs}} - \overline{\mathrm{SM}^{\mathrm{obs}}}\right)\left(\mathrm{SM}_t^{\mathrm{sim}} - \overline{\mathrm{SM}^{\mathrm{sim}}}\right)}{\sqrt{\sum_{t=1}^{n}\left(\mathrm{SM}_t^{\mathrm{obs}} - \overline{\mathrm{SM}^{\mathrm{obs}}}\right)^2 \sum_{t=1}^{n}\left(\mathrm{SM}_t^{\mathrm{sim}} - \overline{\mathrm{SM}^{\mathrm{sim}}}\right)^2}} \tag{10}$$

$$\mathrm{RMSE} = \sqrt{\frac{\sum_{t=1}^{n}\left(\mathrm{SM}_t^{\mathrm{sim}} - \mathrm{SM}_t^{\mathrm{obs}}\right)^2}{n}} \tag{11}$$

$$\mathrm{ubRMSD} = \sqrt{\frac{\sum_{t=1}^{n}\left(\left(\mathrm{SM}_t^{\mathrm{obs}} - \overline{\mathrm{SM}^{\mathrm{obs}}}\right) - \left(\mathrm{SM}_t^{\mathrm{sim}} - \overline{\mathrm{SM}^{\mathrm{sim}}}\right)\right)^2}{n-1}} \tag{12}$$

where n is the total number of time steps, $\mathrm{SM}_t^{\mathrm{sim}}$ the simulated ensemble average soil moisture content at the time step t (either from an open loop (OL) or DA run), and $\mathrm{SM}_t^{\mathrm{obs}}$ the observed soil moisture by CRNS at the time step t. The overbar in Equations 10, 12, and 13 indicates the temporal mean over the study period.

The above performance measures were also used to evaluate the effect of CRNS soil moisture assimilation on evapotranspiration and discharge characteristics simply by replacing soil moisture with evapotranspiration and discharge in the equations.

The Nash-Sutcliffe efficiency (NSE) index was also used to evaluate the simulations of discharge. The NSE was calculated according:

$$\mathrm{NSE} = 1 - \frac{\sum_{t=1}^{n}\left(Q_t^{\mathrm{sim}} - \overline{Q^{sim}}\right)^2}{\sum_{t=1}^{n}\left(Q_t^{\mathrm{obs}} - \overline{Q^{\mathrm{obs}}}\right)^2} \tag{13}$$

where Q_t^{sim} is the simulated ensemble average discharge at the time step t (either from an open loop (OL) or DA run), and Q_t^{obs} is the observed discharge at the time step t. The NSE range is between -∞ and 1. The closer to 1, the more accurate the model is.

4. Results

4.1. Soil Moisture Data Assimilation General Results

Table 4 summarizes the performance in terms of error statistics for OL and different DA experiments (state updates alone and joint state-parameter updates) for 2016 and 2018. For all the DA experiments, both for the wet year 2016 and the dry year 2018, and both for state updating alone and joint state-parameter updating, BIAS,

Table 4
Error Statistics for Open Loop (OL), Data Assimilation With State Updates (State), Joint State-Parameter Updates (Joint), and Jackknife Simulations With Joint State-Parameter Updates (Jackknife) for the Assimilation Periods of 2016 and 2018

Year	Simulation	BIAS (cm^3/cm^3)	MAE (cm^3/cm^3)	R	RMSE (cm^3/cm^3)	ubRMSD (cm^3/cm^3)
2016	OL	−0.051	0.062	0.795	0.077	0.058
	State	−0.024	0.034	0.918	0.044	0.037
	Joint	−0.004	0.023	0.942	0.031	0.031
	Jackknife	−0.012	0.036	0.879	0.046	0.045
2018	OL	0.005	0.054	0.739	0.069	0.069
	State	−0.008	0.032	0.895	0.044	0.043
	Joint	0.001	0.024	0.944	0.033	0.033
	Jackknife	0.008	0.046	0.816	0.058	0.058

Note. The indicators were averaged over all sites with CRNS soil moisture observations. Site-specific indicators are provided in Appendix Tables A1 to A4.

MAE, RMSE, and ubRMSD were lower than for the open loop run, and R was higher than for the OL run, indicating that simulated soil moisture was closer to the measurements after assimilation. Joint state-parameter estimation gave better results than state estimation alone, both in 2016 and 2018. The RMSE of soil moisture decreased by 42.9% (2016) and 36.2% (2018) for state updating only, while for joint state-parameter updates, decreases were 59.7% (2016) and 52.2% (2018). The best assimilation results resulted in similar soil moisture RMSE values for 2016 and 2018, namely 0.031 and 0.033 cm^3/cm^3, respectively. The DA results for two different years illustrate that the effect of CRNS assimilation at the assimilated locations is consistent.

Figures A1 and A2 show the temporal courses of CRNS measured soil moisture, and simulated soil moisture from OL and joint state-parameter estimation in 2016 and 2018 at all the CRNS locations. The figures clearly show that simulated soil moisture for all CRNS sites is closer to measurements after assimilation. The error statistics for all CRNS sites can be found in Tables A1 and A2. The RMSE is less than 0.035 cm^3/cm^3 for most sites (except Wüstebach in 2016, and Rollesbroich and Aachen in 2018), which is within the acceptable range.

For Wüstebach, the RMSE was 0.059 cm^3/cm^3 in 2016, which is still much larger than the measurement error. The scatter plot for Wüstebach in Figure A3 indicates that modeled soil moisture updates reach an upper plafond, which is defined by the maximum possible porosity in the model, which is determined by the soil texture and pedotransfer function. However, the remarkably high porosity of the forest soil is due to the very high content of organic material in the topsoil, so the real porosity of Wüstebach cannot be represented in the model by the soil texture alone (Strebel et al., 2022). Therefore, the upper porosity limit inhibits further improvement of soil moisture characterization. For Rollesbroich, the RMSE was 0.048 cm^3/cm^3 in 2018, and the poor performance is also limited by the porosity, as can be seen in the scatter plot (see Figure A4). As for Aachen, the RMSE was 0.038 cm^3/cm^3 in 2018, and soil moisture simulation might have been negatively impacted by irrigation, which was not accounted for in the model (land use is crop and 2018 was a dry year).

To better understand the effect of the DA during different hydrological conditions, the RMSEs of the SM were also calculated over different seasons (see Appendix Table A5). For DA experiments (both 2016 and 2018), the seasonal SM simulations were obviously improved after assimilation, and joint state-parameter estimation resulted in better performance compared to state update alone. The reduction in RMSE showed small differences across the four seasons in both 2016 and 2018, all ranging from 50% to 60%, suggesting the robustness of DA performance at assimilation locations under different hydrological conditions.

Examples of soil moisture spatial distributions (vertically averaged) for the OL and joint state-parameter estimation runs are shown in Figure 5. The simulated soil moisture for the whole catchment is corrected by data assimilation for both state updates alone and joint state and parameter updates. However, the difference between state assimilation and joint assimilation is small, indicating that parameter update influence is limited. For 2016, a comparison between simulated values from OL and measurements at the CRNS sites revealed that the OL simulation was too dry. Data assimilation corrected the simulations, and in some too dry parts of the catchment, such as grid cells near the river, soil water content increased by assimilation. On the contrary, in 2018, the OL overestimated soil moisture content, and the DA corrected soil moisture toward lower values.

4.2. Jackknife Simulations

In order to investigate whether the limited CRNS stations could improve the simulated soil moisture at locations beyond the CRNS stations over the Rur catchment, 12 jackknife simulations were performed for each year (2016 and 2018). The EnKF may enhance the spatial accuracy of the simulated soil moisture, given the spatial correlation of atmospheric forcings, soil hydraulic parameters, and soil moisture. The overall error statistics of 12 jackknife simulations for 2016 and 2018 are shown in Table 3. Overall, the jackknife runs reduced MAE, RMSE, and ubRMSD, and increased R compared to OL, demonstrating that the soil moisture simulation at verification

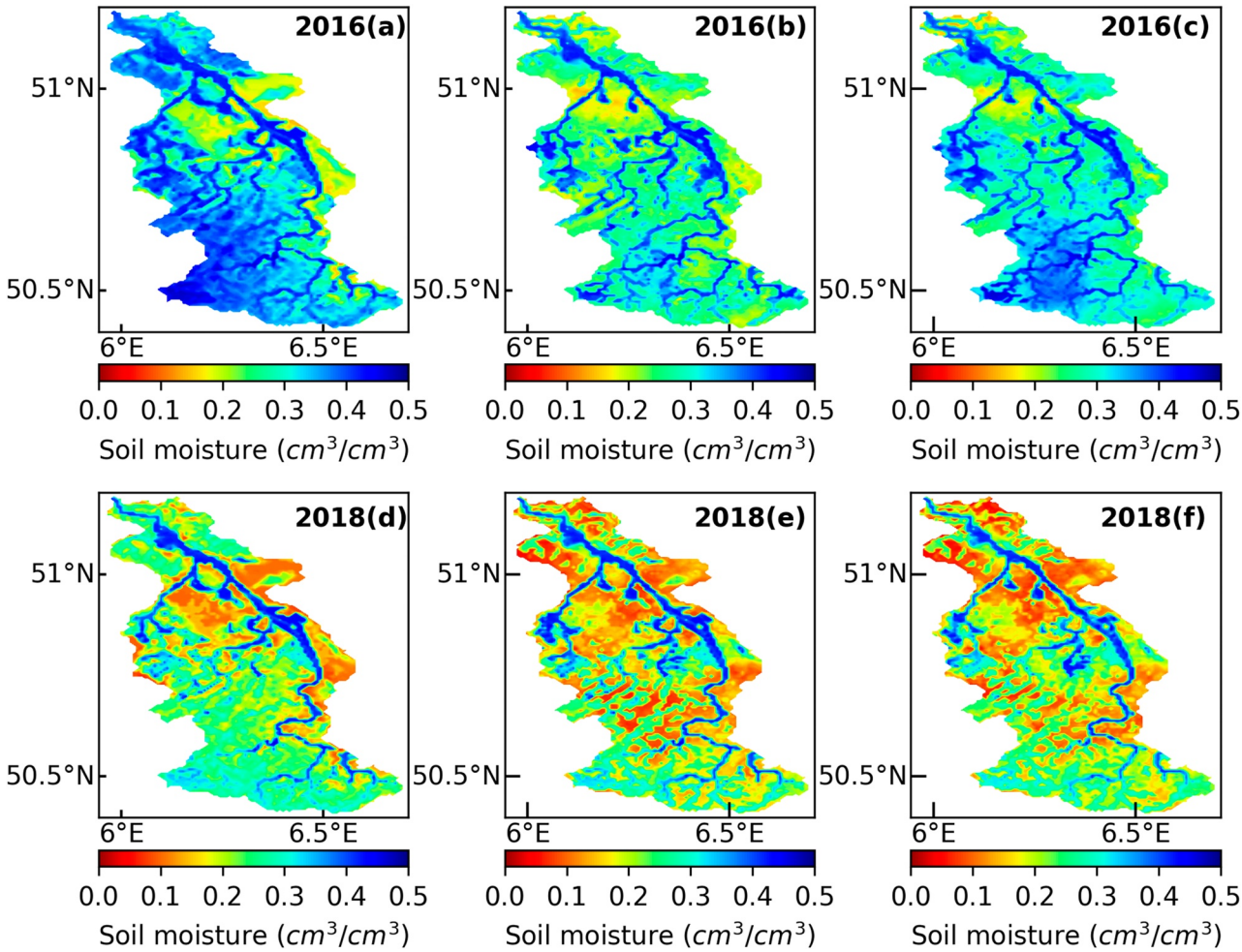

Figure 5. Examples of the simulated soil moisture distribution over the Rur catchment on the 22nd of July in 2016 and 2018. Subplots (a) and (d) are from the open loop, (b) and (e) are from data assimilation with state update, and (c) and (f) are from joint state-parameter update simulations.

locations also improved. On average, the RMSE of the 12 jackknife runs for 2016 was 0.046 cm^3/cm^3, which is much lower than the RMSE for the OL run (0.077 cm^3/cm^3) and only a bit higher than when only the state was updated. For the year 2018, the jackknife simulations resulted in a smaller RMSE reduction at the verification locations, with an average RMSE of 0.058 cm^3/cm^3 (0.069 cm^3/cm^3 for the OL run).

For jackknife runs, the seasonal SM simulations showed quite different performances (see Appendix Table A5), and the extent of RMSE reduction was positively correlated with the average measured SM; the higher the soil moisture content, the larger the RMSE reduction. Therefore, the best performance occurred during the winter, when soil moisture was at its maximum for the whole year (47.7% and 34.3% RMSE reduction for 2016 and 2018, respectively). The worst performance was found for dry soil water conditions, for example, 32.3% RMSE reduction in autumn 2016. In 2018, the extreme dry conditions in the summer even led the RMSE to increase by 8.8%.

For each CRNS site, the jackknife simulation performed differently in 2016 and 2018 (see Figures A5 and A6). More detailed site statistics can be found in Tables A3 and A4. For 2016, all jackknife simulations resulted in an improved RMSE at the verification locations compared to the OL run. Assimilation could reduce RMSE by 70% at sites with a high RMSE in the OL run, such as Aachen (see Figure 6). In 2018, the RMSE for Aachen decreased by 36%, but RMSE reductions were smaller at other sites (for Gevenich, Heinsberg, and Schönseiffen, the RMSE even increased after assimilation). For Heinsberg, the RMSE for the DA-run in 2018 is higher (0.057 cm^3/cm^3) than for the OL-run (0.044 cm^3/cm^3), while the RMSE value decreased by 35% in 2016 (see Figure 6). Figure A7 shows the spatial correlation of soil moisture from OL between the CRNS locations (Gevenich, Heinsberg, and Schönseiffen) and other grid cells in the catchment on a specific day in the summer. The figure indicates that the

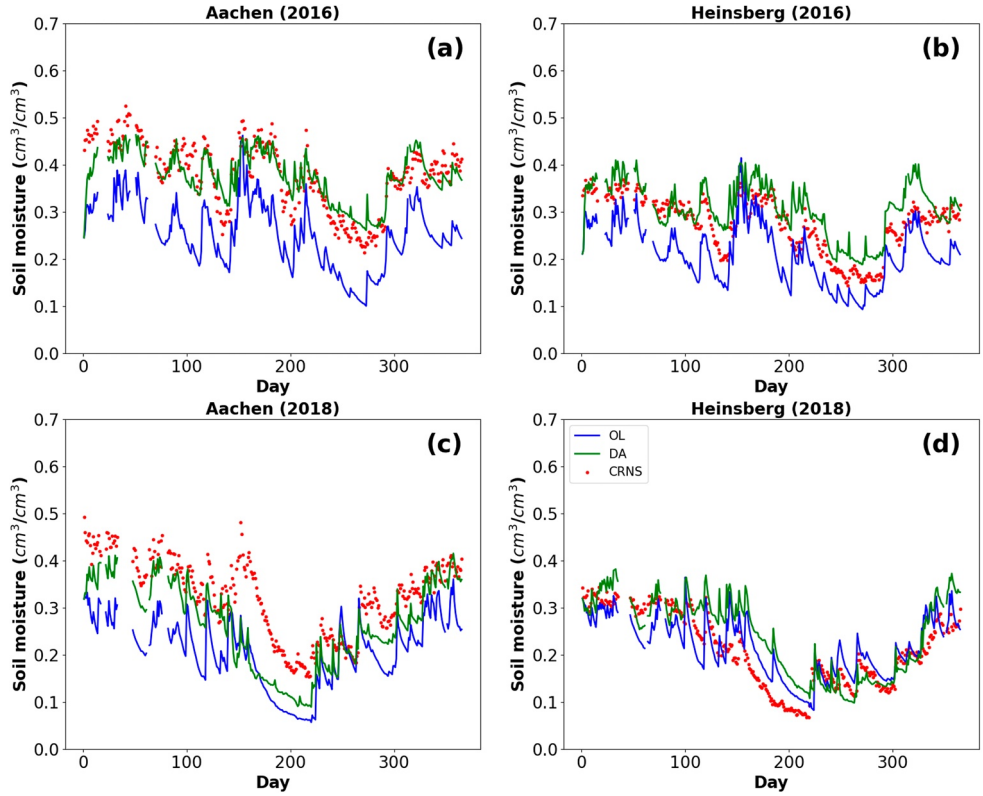

Figure 6. Temporal evolution of simulated soil moisture from the open loop mean (OL, blue) and jackknife simulation mean (DA, green), together with the observed soil moisture from the CRNS (red), for 2016 (a), (b) and 2018 (c), (d) at the CRNS sites. Simulated soil moisture was vertically weighted using the revised method by Schrön et al. (2017).

spatial correlation around the CRNS locations was weaker in 2018 (dry) compared to 2016 (wet), which resulted in less accurate jackknife simulations in 2018 compared to 2016.

4.3. Temporal Evolution of Parameter Estimates and Parameter Verification

The temporal evolution of K_s estimates during the assimilation period (2016 and 2018) for the CRNS sites is shown in Figure 7. Once the assimilation began, the parameters varied considerably within short time intervals. For most sites, the updated K_s started to stabilize after about 100 days of assimilation. Compared to the initial input K_s, most sites showed a decreasing trend during assimilation, while only Rollesbroich in 2016 showed a slightly increasing trend. The changing values for K_s estimates for Merzenhausen, Gevenich, Ruraue, Heinsberg, Selhausen, and Kleinhau were remarkably consistent for the two distinct assimilation years.

The years 2016 and 2018 resulted in very similar parameter sites, with differences smaller than 0.10 $\log_{10}$ (m/s) units at the end of the assimilation period for more than half of the sites (Figure 7). Some sites like Gevenich and Kall showed only slight variations from the prior values, with K_s changes less than 0.20 $\log_{10}$ (m/s) units, while for Ruraue and Wüstebach K_s changed more than 0.45 $\log_{10}$ (m/s) units. Among all sites, Wildenrath has the largest absolute variation, with K_s varying more than 10^{-5} m/s, while Kall showed very small variations, with absolute K_s changes less than $5*10^{-7}$ m/s. Temporally unstable and inconsistent parameter estimates imply that there may be multiple or seasonal optimal parameter values, so the fluctuations in K_s may be related to variations in atmospheric forcings. Some instability in the updated parameters could also be related to the compensation for other errors, for example, errors in the inputs (from atmospheric forcings or soil hydraulic parameters) and model structural errors.

Figure 8 depicts the prior and updated spatial ensemble mean of $\log K_s$ at 2 cm depth (similar pattern for depths up to 80 cm), both for the years 2016 and 2018. Assimilation had a noticeable impact on K_s, particularly around the assimilated CRNS measurement locations, resulting in a decrease in its overall value. The $\log K_s$ changes for the

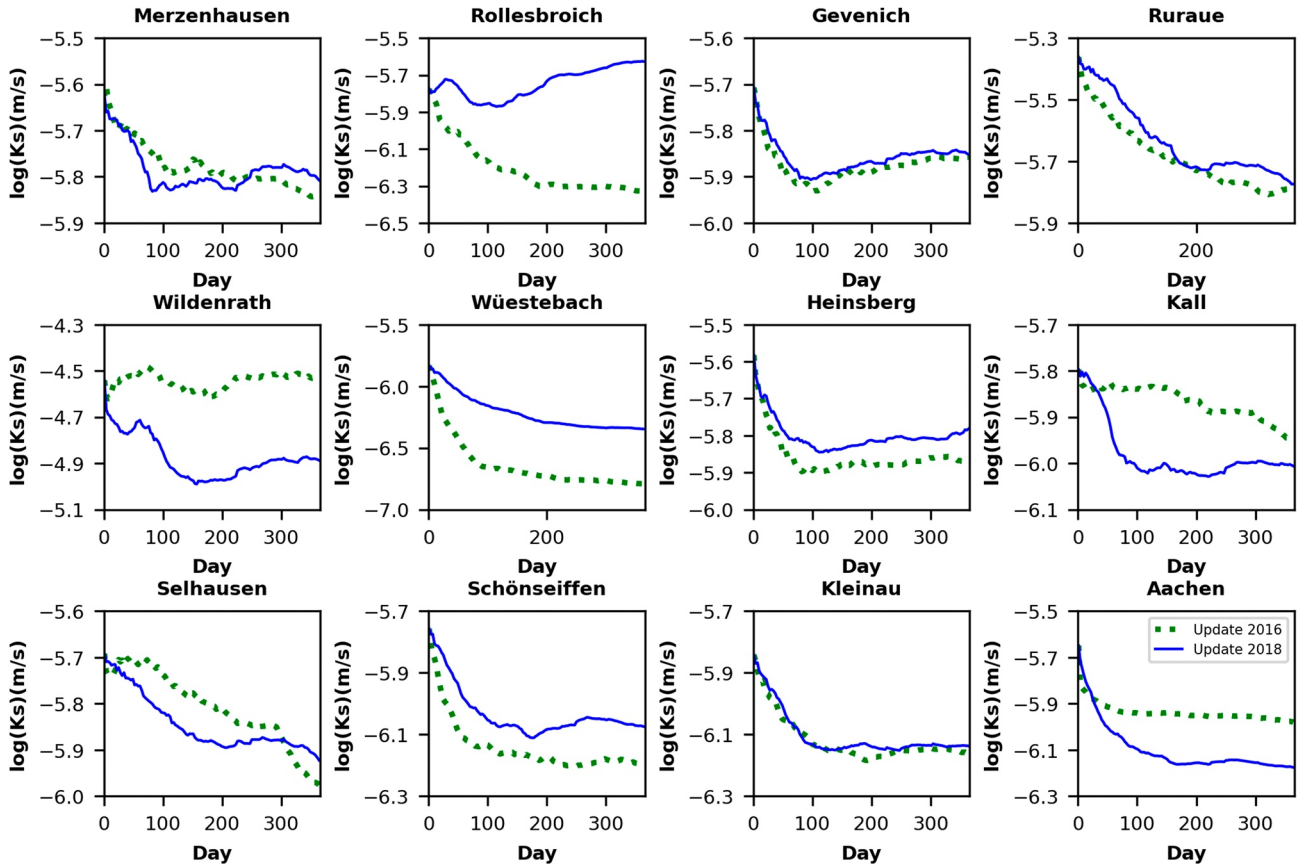

Figure 7. Estimates of averaged saturated hydraulic conductivity ($\log_{10}K_s$) from data assimilation experiments with joint state-parameter updating during the periods of 2016 and 2018 at CRNS locations. The input value of K_s is indicated at the first time step.

simulation year 2016 were more noticeable than for 2018. The reason for the larger $\log K_s$ updates in 2016 could be that the simulated soil moisture content by the OL was lower than the observed values. 2018 was a particularly dry year, so the soil moisture condition in 2018 was closer to that of OL than in 2016, resulting in a larger update of the $\log K_s$ in 2016 than in 2018. Grids with larger distances to the CRNS sites show smaller $\log K_s$ updates because of the weak correlations with the soil moisture observations. Additionally, there are some grid cells with increased $\log K_s$ after data assimilation, suggesting that horizontal water redistribution, for example, due to lateral groundwater flow or surface runoff, resulted in different $\log K_s$ changes than at the CRNS sites.

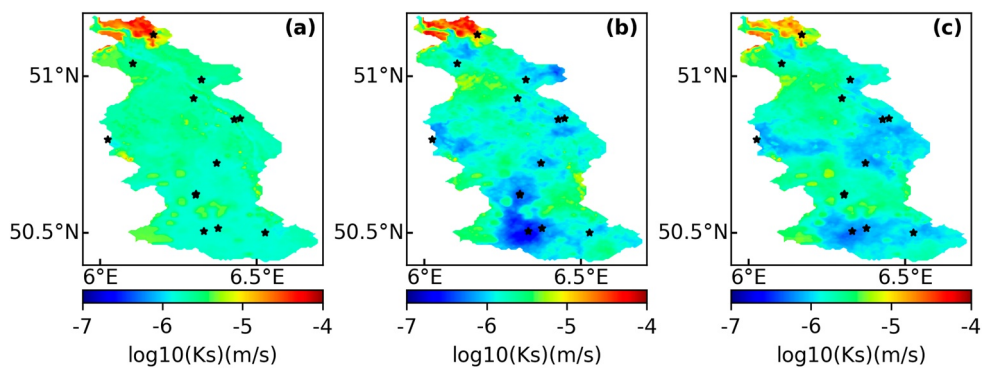

Figure 8. Ensemble averaged $\log_{10}K_s$ fields of the soil at 2 cm depth: (a) prior field; (b) DA with joint state-parameter updates at the end of 2016; (c) DA with joint state-parameter updates at the end of 2018. The black asterisk is the location of the CRNS sites.

Table 5
Comparison of Measured and Simulated Soil Moisture for the Year 2017 (Evaluation Period, No Assimilation)

Simulation	BIAS (cm^3/cm^3)	MAE (cm^3/cm^3)	R	RMSE (cm^3/cm^3)	ubRMSD (cm^3/cm^3)
OL	−0.019	0.051	0.733	0.066	0.063
Updated K_s from 2016	−0.007	0.047	0.769	0.060	0.059
Updated K_s from 2018	−0.012	0.049	0.760	0.061	0.060

Note. The updated parameters used for verification were from the assimilation period (2016 and 2018). The error statistics were averaged over all CRNS sites.

Simulations were made for the verification year 2017, using as input updated hydraulic parameters from either 2016 or 2018. For the verification year, reduced BIAS, MAE, RMSE, and ubRMSD, and a small increase in R compared to OL were found (see Table 5). Using the updated K_s from the 2016 simulation as input to the simulation for the year 2017 gave simulated soil moisture contents that were closer to observations than when the updated K_s from the 2018 simulation were used as input. The updated parameter's verification for the year 2018 was less successful than for the year 2016, which may be due to the hydrological conditions during 2016 (average CRNS soil moisture 0.31 cm^3/cm^3) being more similar to 2017 (0.29 cm^3/cm^3), as 2018 (0.26 cm^3/cm^3) was a dry year.

4.4. Evapotranspiration and Discharge

The effect of soil moisture DA on ET modeling was also investigated. We used observed ET data from three EC stations for comparison with simulated values in order to examine the impact of CRNS soil moisture assimilation on ET simulations. Results of the DA experiments showed that soil moisture states were significantly altered, and ET was also somewhat impacted by the different assimilation scenarios, depending on the simulation year (see Table A6). Moreover, the joint state-parameter assimilation resulted in a better ET prediction than soil moisture state updating alone.

The statistical performance measures BIAS, MAE, R, RMSE, and ubRMSD, comparing simulated ET (by OL and joint state-parameter updates) and EC data, are provided in Table 6. These statistical measures were computed on a monthly basis, as the parameter LAI in the CLM model is provided on a monthly scale. The joint state-parameter updates with CRNS soil moisture assimilation showed lower BIAS, MAE, and RMSE values than OL, except for Rollesbroich in 2018, demonstrating that ET simulation improved if soil moisture simulation was improved by data assimilation. However, the relative improvement in the characterization of ET is far smaller than for soil moisture. The high correlation coefficients (larger than 0.95) for Rollesbroich and Wüstebach, either for OL or DA, indicate a good fit between simulated and measured ET, mainly because of the reproduction of the yearly cycle. For Selhausen, the correlation is lower (less than 0.85), which might be related to different crops being cultivated for the years 2016 and 2018 (winter barley in 2016 and winter wheat in 2018). CLM uses the same parameters for these crops, and for example, the harvest date is not well represented by the model. For Rollesbroich, the ET simulation in 2018 was worse after DA (compared to OL) because the overestimated soil moisture in the OL run was corrected toward lower values, reducing ET, which further exacerbated the ET underestimation.

Table 6
Comparison of Measured and Simulated Evapotranspiration (Monthly) and Discharge (Monthly) From Open Loop (OL) and Data Assimilation Runs With Joint State-Parameter Updates (DA) for Two Assimilation Periods (2016 and 2018)

		BIAS (mm/month)		MAE (mm/month)		R		RMSE (mm/month)		ubRMSD (mm/month)	
Year	Site	OL	DA	OL	DA	OL	DA	OL	DA	OL	DA
2016	Rollesbroich	−10.17	−8.02	10.31	8.75	0.98	0.97	12.97	10.79	8.05	7.22
	Wüstebach	−17.93	−16.05	17.93	16.36	0.99	0.99	21.48	19.41	11.82	10.91
	Selhausen	−14.11	−7.27	15.77	12.37	0.87	0.85	18.53	14.63	12.02	12.69
2018	Rollesbroich	−12.77	−14.26	13.68	15.22	0.97	0.97	18.05	19.86	12.76	13.83
	Wüstebach	−11.46	−10.50	13.36	12.33	0.96	0.95	17.24	16.25	12.88	12.40
	Selhausen	−8.14	−3.87	16.33	14.02	0.80	0.81	20.66	18.73	18.99	18.32
		BIAS (m^3/s)		MAE (m^3/s)		R		RMSE (m^3/s)		NSE	
Year	Site	OL	DA	OL	DA	OL	DA	OL	DA	OL	DA
2016	Erkensruhr-Einruhr	−0.23	−0.23	0.32	0.31	0.85	0.86	0.48	0.46	0.62	0.64
2018	Erkensruhr-Einruhr	−0.15	−0.16	0.27	0.27	0.90	0.86	0.41	0.41	0.67	0.69

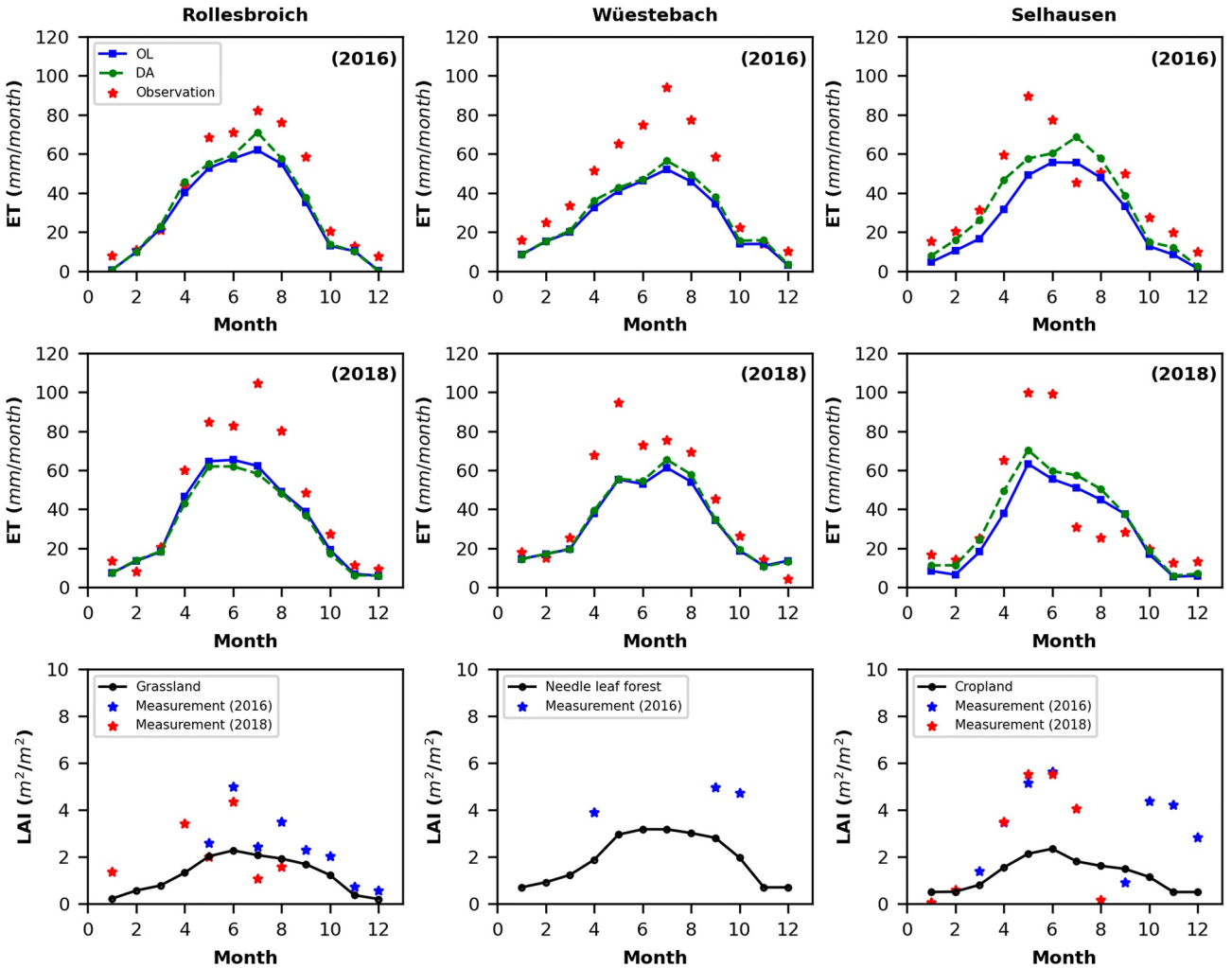

Figure 9. Temporal evolution of simulated evapotranspiration from open loop (OL, blue), data assimilation (joint state-parameter updates, DA, green), and the observed evapotranspiration (red) at the sites Rollesbroich, Wüstebach, and Selhausen for the assimilation periods of 2016 (first row) and 2018 (second row). Monthly Leaf Area Index for the plant functional types at the sites Rollesbroich (grassland), Wüstebach (needle leaf forest), and Selhausen (cropland), as well as the available daily LAI measurements from 2016 to 2018 (third row).

Figure 9 shows the monthly temporal ET variations for the OL run and the joint state-parameter experiment, compared to the EC data. The simulated ET tends to be closer to the observed values after soil moisture assimilation, and the larger changes in ET simulation are observed during drier conditions, specifically in the summer, which is consistent with the results by Hung et al. (2022). For example, for Rollesbroich (2016) and Wüstebach (2018), the largest reductions in RMSE for ET occur in the summer, with 11.5% and 5.4%, respectively. However, for Wüstebach (2016), RMSE decreased most in the autumn, with 9.5%. For Selhausen, the largest RMSE reduction in ET occurred in the spring, for both 2016 and 2018, with reductions of 27.8% and 22.2%, respectively. In the winter, ET simulations hardly improved for Rollesbroich and Wüstebach. ET is limited by available energy under conditions of high SM, so SM changes have a minimal impact on ET. Therefore, the overall ET improvement for the entire year is limited.

The annual ET for 2016 and 2018 across the whole Rur catchment for OL and joint state-parameter updating are presented in Figure 10. Since the ET changes were minimal in the assimilation experiments, only results for joint state-parameter updating are shown. For the OL simulation, the ET in 2018 was greater than in 2016, mainly due to the significantly higher temperature and higher incoming shortwave radiation in 2018, and in spite of the drier conditions. Data assimilation did not much affect simulated ET in the southern part of the catchment, where ET was generally energy limited. In contrast, simulated ET in the northern part of the catchment with generally

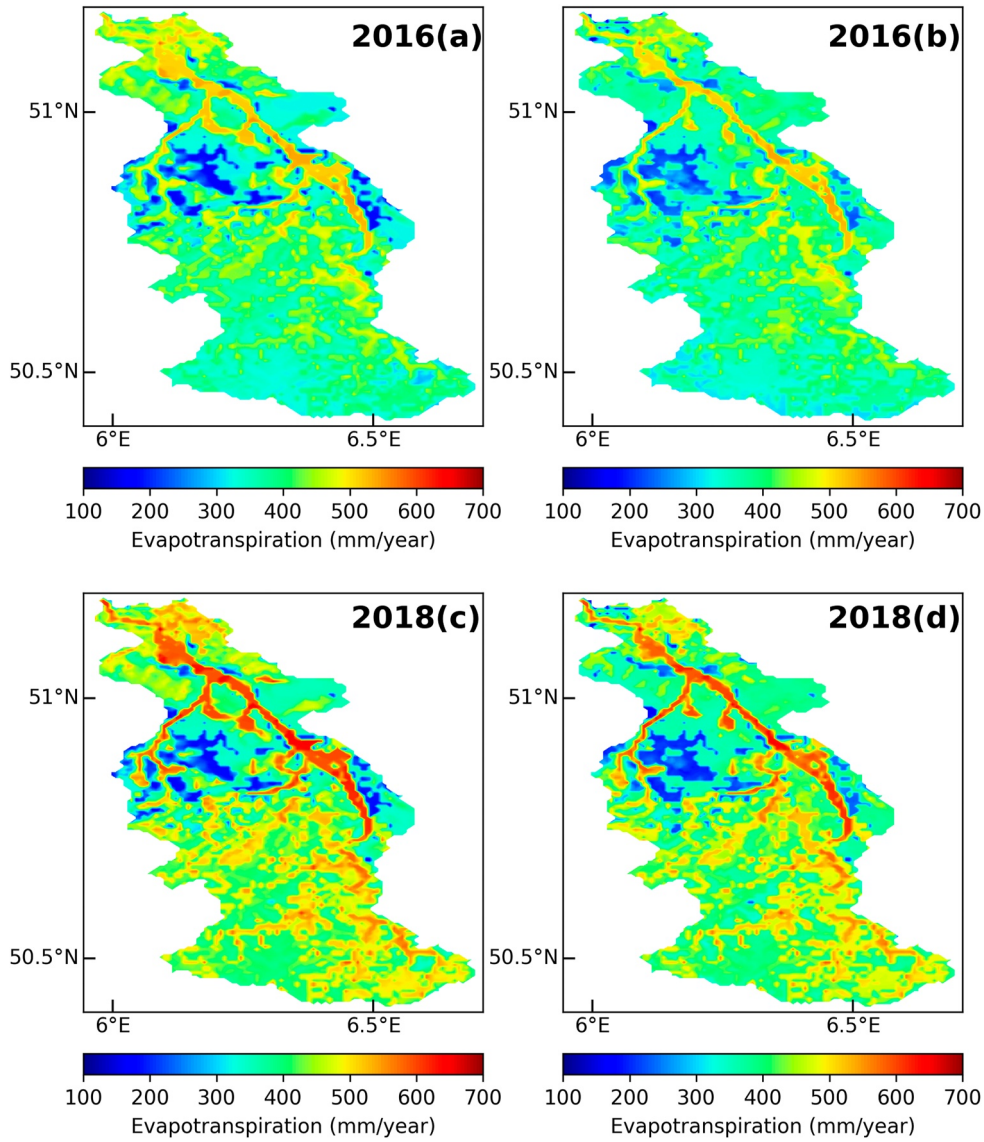

Figure 10. Annual evapotranspiration from open loop (a), (c) and DA runs (joint state-parameter updates) (b), (d) over the Rur catchment during the assimilation periods.

less precipitation was affected by DA, with ET increases of more than 50 mm yr^{-1} for many grid cells in 2016, whereas ET was modified less by DA in 2018. This is related to the larger update of soil hydraulic parameters in 2016 compared to 2018.

Figure 11 compares the simulated river discharge from the OL and DA experiments to the discharge from the in situ station Erkensruhr-Einruhr (indicated in Figure 1). This sub-catchment was hardly affected by water management operations, so it was selected. For comparison purposes, the SM data of the CRNS station in Wüstebach are also shown since it is located in the catchment area of the Erkensruhr-Einruhr station. For the sake of simplicity, only the results of the joint state-parameter update are shown, as the results for the other experiments are very similar. The coupled model performance for discharge simulation is satisfactory, as the NSEs of 2016 and 2018 were 0.62 and 0.64, respectively. The simulated discharge could capture the daily variations, including discharge peaks (see Figure 11). DA only slightly improves monthly discharge estimation compared to the OL (see Table 6), with an increase in NSE of about 0.02 for both 2016 and 2018, even though SM in Wüstebach was significantly improved by DA.

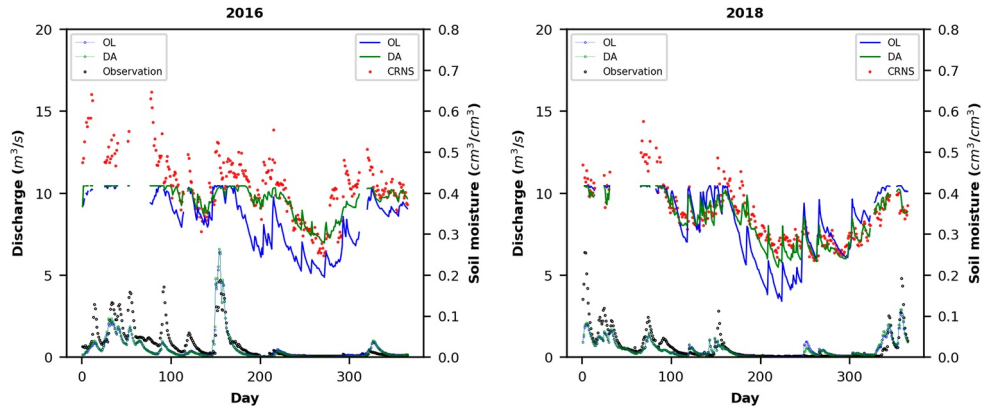

Figure 11. Temporal evolution of simulated discharge from the open loop mean (OL, blue circle) and joint state-parameter assimilation mean (DA, green circle), together with the observed discharge (black circle) for 2016 and 2018 at the Erkensruhr-Einruhr in situ station. The temporal evolution of simulated soil moisture from the open loop mean (OL, blue line) and joint state-parameter assimilation mean (DA, green line), together with the observations (red dot) for 2016 and 2018 at the Wüstebach site.

4.5. Discussion

This study demonstrated that the assimilation of CRNS soil moisture data is beneficial and improves the integrated terrestrial system model simulations of soil moisture over a real catchment, both for a wet and dry year. In addition, the jackknife simulations demonstrate the potential of the CRNS network to improve modeled soil moisture at the catchment scale, but it performs differently in a wet and dry year. The improvement in the dry year is relatively small, due to the weaker spatial correlations in the dry year 2018, compared to the wet year 2016. The same perturbation methods were used for the 2 years and the spatial correlation length utilized for soil hydraulic parameter perturbations ensured that each site used for validation was within the correlation length of the assimilated sites. However, the soil moisture spatial correlation fluctuated under various soil hydrological conditions and was shown to be weakened under drought conditions. As a result, the drought in the summer of 2018 led to the worst validation performance of the seasonal SM simulation. The overall results from the jackknife experiments also indicate that the RMSE is much less reduced at the verification locations than at the assimilation locations.

It is very likely that a denser CRNS network may improve soil moisture characterization, for example, related to better parameter estimates and compensate for variations in performance across years. To further investigate how dense an optimal measurement network of CRNS should be, one possible approach could involve conducting a synthetic study that tests varying numbers and locations of CRNS stations based on the model results established in this study. In addition, some denser CRNS observation networks are gradually being established, such as the new Irish Soil Moisture Observation Network (ISMON) (Finkele et al., 2022) and some field campaigns in which a large number of CRNS were operated together to explore the potential of a dense stationary CRNS network to monitor spatio-temporal SM dynamics at the catchment scale. For instance, a dense network of 24 CRNS was established in an area of only 1 km^2 in the pre-alpine Rott headwater catchment in southern Germany (Fersch et al., 2020) and a network of 15 CRNS covering an area of 0.39 km^2 in the Wüstebach headwater catchment in western Germany (Heistermann et al., 2022). In our study, we show the potential high-density CRNS networks have to correct for errors introduced by imperfect input data and spatial correlations, thus reducing the uncertainties in SM prediction. The establishment of the above-mentioned CRNS observation networks offers the opportunity to further investigate how the density of sensors influences SM assimilation.

Joint state-parameter estimating improved soil moisture simulations, especially at measurement locations, but much less at verification locations. Hydraulic conductivity was only modified slightly and locally during joint state-parameter updating, and as a result, soil moisture characterization only improved slightly. Better results could be achieved with a larger ensemble size. Here, data assimilation experiments were performed with 128 ensemble members, but this ensemble size might still be too small. Hendricks Franssen and Kinzelbach (2008) suggested that 200–500 realizations are needed to achieve successful joint state-parameter estimation with

groundwater hydrological models. A larger ensemble size, however, was not feasible in this work, given the needed compute time for a run with the high-resolution integrated model.

DA reduced differences between simulated and measured soil moisture contents significantly, but the benefit of DA was not clear for the modeling of ET, and the findings are in line with the synthetic study by Hung et al. (2022) with the TSMP-PDAF model. Similar findings were made by Ridler et al. (2014), who found that soil moisture assimilation had little influence on flux estimation. Uncertain parameters and model structural errors are also possible reasons for the limited improvement in ET simulations after soil moisture assimilation.

It is important to note that more studies have reported the underestimation of evapotranspiration (or latent heat flux) by CLM (Boas et al., 2021; Shrestha et al., 2014). The ET mismatch in our simulations was largely related to a systematic underestimation of ET (bias), which seems partly related to underestimated LAI values. The input LAI used in this study was taken from previous studies (Sulis et al., 2015, 2018), but was found to be smaller than the measured LAI values at EC sites (see Figure 9). Notice that the measured LAI is on a daily basis, while the LAI in the model is defined on a monthly basis, but the systematic underestimation of the LAI in the model can nevertheless be observed.

The performance of the ET simulation is also affected by the use of a uniform set of parameters for crops, neglecting the fact that different crops in the region can have very different properties (e.g., LAI and stem area index). Sulis et al. (2015) incorporated crop-specific parameters in CLM3.5 simulations, which resulted in improved simulations of land-atmosphere exchange fluxes compared to simulations using the generic crop type. Similarly, a more recent study by Boas et al. (2021) found that utilizing crop-specific parameters in the newer version 5.0 of CLM improved the representation of crop growth cycles and led to more accurate simulations of energy fluxes. The model CLM5 shows a better characterization of ET than CLM3.5 (Shrestha, Kurtz, et al., 2018), but it is not yet coupled to ParFlow, which is the reason why we did not use it in this work. In addition, other factors influence ET, like vegetation rooting depth and further vegetation characteristics (Li et al., 2020). The uncertainty of those parameters was not considered in this work, but in order to improve ET simulation in DA studies, their uncertainty should be considered in the future. Finally, mismatches between modeled and measured ET are probably also related to errors in the input of atmospheric forcings like incident radiation. A fully coupled atmosphere-land surface-subsurface model integrated into the DA framework may further improve the characterization of ET.

Therefore, it can be concluded that assimilating only soil moisture is insufficient to significantly improve the simulation of ET and that parameter biases and model errors are more important for the ET simulation. Better results may be achieved by assimilating additional types of measurements, like LAI, and estimating further parameters, like vegetation parameters.

River discharge was used to investigate the effects of SM assimilation on lateral fluxes, with slight improvements in discharge estimates. Our finding is consistent with previous synthetic SM assimilation experiments at the hillslope or larger catchment scale using the integrated model TSMP (Gebler et al., 2019; Hung et al., 2022). The limited improvement in discharge characterization may be attributed to the limited spread of discharge and to the fact that only the soil hydraulic parameter K_s was updated without large changes in the parameter values. On the other hand, the limited improvement might also be partly related to model structural errors (e.g., underrepresentation of preferential flows and representation of drainage) (Gebler et al., 2019). Furthermore, Baroni et al. (2017) found that river discharge in large catchments is only sensitive to the perturbation of long spatial structures and is not affected by small-scale soil variabilities. Therefore, with only SM and parameter K_s being updated in the integrated model, an improvement in the performance of discharge estimation is challenging. Possible improvements could be achieved by considering the uncertainties in other parameters. For instance, D. Baatz et al. (2017) found that the estimated Manning's roughness coefficients could improve the discharge simulation with TSMP in synthetic 2D experiments.

In this study, we did not directly assimilate the CRNS neutron intensity observations but used soil moisture products derived from the CRNS observations. Next, it is planned to assimilate neutron count intensity directly with the COSMIC operator (Shuttleworth et al., 2013). In addition, although we used a 500-m resolution, which is already fine relative to the remote sensing data, 500-m is still coarse compared to the footprint of CRNS data. Therefore, a higher resolution will be used in the future to include the calculation of the horizontal weighting of the CRNS observations.

Our study demonstrates the potential of a CRNS observational network to enhance SM estimation as well as other hydrological variables (evapotranspiration and discharge) at a larger catchment scale, suggesting promising prospects for the application of CRNS compared to traditional SM sensors or RS data sets. The footprint of CRNS covers areas with a diameter of 300–600 m and a depth of 15–70 cm, which is much larger than the measurement volume of conventional SM measurement methods such as point-type soil moisture sensors. Remote sensing data can provide spatially continuous SM information, but typically only for the top soil (0–5 cm). Therefore, the SM data from CRNS better represent the scale of model grids and thus can provide more accurate parameters for hydrological models to simulate hydrological processes such as infiltration, evapotranspiration, and runoff. We have also shown that the assimilation of SM from CRNS can improve SM estimates in the vicinity as well as at distant locations from CRNS stations. This indicates that even a low number of CRNS can provide useful information for data assimilation. For instance, Patil et al. (2021) demonstrated that assimilating SM from four CRNS improved SM simulation in a 655 km^2 catchment. This suggests that the use of CRNS instead of point sensors could reduce the number of measuring stations, which in turn may reduce installation and maintenance costs.

5. Conclusions

Soil moisture measurements from 12 CRNS distributed over the Rur catchment (~2,400 km^2) were assimilated into TSMP with EnKF. This is the first application of the assimilation of observed soil moisture data from CRNS into an integrated land surface-subsurface model for a real-world case. To this end, 128 ensemble members were generated by considering uncertain atmospheric forcings and subsurface hydraulic parameters. DA experiments were conducted for a wet year (2016) and a dry one (2018), with state-only updates and joint updates of state and parameters. Soil moisture observations from CRNS, evapotranspiration from eddy covariance stations, and discharge from an in situ station were used as validation data to assess the impact of soil moisture assimilation on soil moisture and flux simulation. EnKF assimilation of soil moisture from CRNS improves soil moisture estimation at measurement sites strongly in both dry and wet years, with up to 60% RMSE reductions. Joint state-parameter estimation results in a slightly better soil moisture simulation than state estimation alone, with an RMSE reduction of more than 15% compared to state estimation alone. Jackknife experiments show limited improvement in soil moisture characterization at independent verification locations, and the verification performance is affected by hydrological conditions, showing worse performance in dry episodes, indicating that the measurement network (~1 site per 200 km^2) is not dense enough. Soil moisture assimilation improved ET and discharge characterization to a much lesser degree than soil moisture, indicating limited sensitivities of ET and discharge toward soil moisture.

The DA experiments show that improving the characterization of states (spatially and temporally) in the integrated surface-subsurface model TSMP by assimilating SM from a distributed CRNS network at the catchment scale is challenging but also promising. Compared to RS and traditional point SM measurements, CRNS could provide larger-scale in-situ SM data with high temporal resolution and deeper penetration depth. In combination with DA, a limited number of sensors makes it feasible to continuously and stably determine SM dynamics from the field to the catchment scale. Better SM information is important for improving our understanding of the processes in terrestrial water cycles and reducing the large uncertainties of hydrological fluxes during modeling. Large-scale networks of CRNS already exist in the USA, Europe, Australia and India, but the density of sensors is still not sufficient to completely represent soil moisture patterns at the continental scale. As sensors become more affordable, higher observational coverage will become possible, enabling the acquisition of long-term SM data sets to monitor climate change and support predictions.

To improve the characterization of the states and parameters of integrated land surface-subsurface simulation at large scales, in addition to assimilating soil moisture from a denser CRNS measurement network, future work should focus on multivariate assimilation (e.g., joint assimilation with vegetation related data) and the estimation of further soil hydraulic and vegetation parameters with integrated terrestrial system models at a higher spatial resolution.

10.1029/2023WR035056

Appendix A

Table A1
Comparison of CRNS Soil Moisture Measurements and Simulated Soil Moisture From Open Loop (OL) and Data Assimilation With Joint State and Parameter Updating (DA) for the Year 2016

	BIAS (cm^3/cm^3)		MAE (cm^3/cm^3)		R		RMSE (cm^3/cm^3)		ubRMSD (cm^3/cm^3)	
Site	OL	DA	OL	DA	OL	DA	OL	DA	OL	DA
Merzenhausen	−0.036	0.001	0.041	0.022	0.870	0.902	0.048	0.029	0.032	0.028
Rollesbroich	−0.010	−0.009	0.036	0.026	0.854	0.957	0.044	0.032	0.043	0.030
Gevenich	−0.050	0.016	0.055	0.023	0.879	0.949	0.063	0.030	0.038	0.025
Ruraue	−0.074	−0.019	0.075	0.025	0.779	0.936	0.084	0.030	0.041	0.023
Wildenrath	−0.012	−0.003	0.024	0.015	0.856	0.902	0.030	0.021	0.028	0.021
Wüstebach	−0.083	−0.033	0.084	0.042	0.731	0.797	0.097	0.059	0.051	0.049
Heinsberg	−0.064	0.003	0.065	0.017	0.854	0.928	0.072	0.023	0.033	0.023
Kall	0.014	0.000	0.031	0.020	0.886	0.946	0.037	0.024	0.034	0.024
Selhausen	−0.120	−0.011	0.121	0.026	0.852	0.906	0.127	0.035	0.040	0.033
Schönseiffen	−0.050	0.008	0.057	0.022	0.843	0.930	0.067	0.027	0.045	0.025
Kleinau	0.002	−0.005	0.027	0.023	0.915	0.947	0.035	0.028	0.034	0.028
Aachen	−0.126	−0.009	0.126	0.022	0.883	0.920	0.130	0.030	0.034	0.028

Table A2
Comparison of CRNS Soil Moisture Measurements and Simulated Soil Moisture From Open Loop (OL) and Data Assimilation With Joint State and Parameter Updating (DA) for the Year 2018

	BIAS (cm^3/cm^3)		MAE (cm^3/cm^3)		R		RMSE (cm^3/cm^3)		ubRMSD (cm^3/cm^3)	
Site	OL	DA	OL	DA	OL	DA	OL	DA	OL	DA
Merzenhausen	0.025	0.000	0.042	0.023	0.786	0.937	0.056	0.030	0.050	0.030
Rollesbroich	0.045	0.019	0.060	0.039	0.794	0.874	0.072	0.048	0.055	0.044
Gevenich	0.003	0.004	0.043	0.026	0.785	0.929	0.053	0.034	0.053	0.034
Ruraue	−0.015	−0.015	0.056	0.024	0.711	0.957	0.066	0.030	0.064	0.026
Wildenrath	0.021	0.001	0.028	0.014	0.892	0.943	0.035	0.021	0.028	0.021
Wüstebach	−0.017	−0.014	0.049	0.024	0.702	0.886	0.062	0.033	0.060	0.030
Heinsberg	0.007	0.005	0.037	0.017	0.833	0.959	0.044	0.024	0.044	0.024
Kall	0.072	0.014	0.073	0.024	0.812	0.926	0.086	0.034	0.047	0.031
Selhausen	−0.031	0.006	0.051	0.025	0.780	0.939	0.064	0.031	0.056	0.031
Schönseiffen	0.015	0.007	0.036	0.023	0.908	0.950	0.045	0.028	0.043	0.028
Kleinau	0.061	0.005	0.062	0.025	0.875	0.953	0.076	0.032	0.046	0.032
Aachen	−0.113	−0.018	0.115	0.028	0.810	0.917	0.123	0.038	0.049	0.033

Table A3
Comparison of CRNS Soil Moisture Measurements and Simulated Soil Moisture From Open Loop (OL) and Jackknife Simulations (DA) for the Year 2016

	BIAS (cm^3/cm^3)		MAE (cm^3/cm^3)		R		RMSE (cm^3/cm^3)		ubRMSD (cm^3/cm^3)	
Site	OL	DA	OL	DA	OL	DA	OL	DA	OL	DA
Merzenhausen	−0.036	−0.022	0.041	0.031	0.870	0.846	0.048	0.039	0.032	0.032
Rollesbroich	−0.010	−0.017	0.036	0.030	0.854	0.912	0.044	0.038	0.043	0.034

Table A3
Continued

Site	BIAS (cm^3/cm^3)		MAE (cm^3/cm^3)		*R*		RMSE (cm^3/cm^3)		ubRMSD (cm^3/cm^3)	
	OL	DA	OL	DA	OL	DA	OL	DA	OL	DA
Gevenich	−0.050	−0.022	0.055	0.037	0.879	0.889	0.063	0.046	0.038	0.040
Ruraue	−0.074	−0.039	0.075	0.042	0.779	0.936	0.084	0.047	0.041	0.026
Wildenrath	−0.012	−0.015	0.024	0.023	0.856	0.891	0.030	0.029	0.028	0.025
Wüstebach	−0.083	−0.076	0.084	0.076	0.731	0.859	0.097	0.085	0.051	0.039
Heinsberg	−0.064	0.033	0.065	0.038	0.854	0.839	0.072	0.047	0.033	0.033
Kall	0.014	0.004	0.031	0.028	0.886	0.874	0.037	0.036	0.034	0.035
Selhausen	−0.120	−0.015	0.121	0.039	0.852	0.832	0.127	0.050	0.040	0.047
Schönseiffen	−0.050	0.033	0.057	0.040	0.843	0.901	0.067	0.047	0.045	0.033
Kleinau	0.002	−0.005	0.027	0.026	0.915	0.909	0.035	0.034	0.034	0.033
Aachen	−0.126	−0.002	0.126	0.030	0.883	0.848	0.130	0.039	0.034	0.039

Table A4
Comparison of CRNS Soil Moisture Measurements and Simulated Soil Moisture From Open Loop (OL) and Jackknife Simulations (DA) for the Year 2018

Site	BIAS (cm^3/cm^3)		MAE (cm^3/cm^3)		*R*		RMSE (cm^3/cm^3)		ubRMSD (cm^3/cm^3)	
	OL	DA	OL	DA	OL	DA	OL	DA	OL	DA
Merzenhausen	0.025	0.041	0.042	0.043	0.786	0.904	0.056	0.054	0.050	0.035
Rollesbroich	0.045	0.019	0.060	0.040	0.794	0.873	0.072	0.048	0.055	0.044
Gevenich	0.003	0.019	0.043	0.052	0.785	0.773	0.053	0.063	0.053	0.060
Ruraue	−0.015	−0.041	0.056	0.045	0.711	0.919	0.066	0.055	0.064	0.036
Wildenrath	0.021	0.007	0.028	0.027	0.892	0.835	0.035	0.034	0.028	0.034
Wüstebach	−0.017	−0.044	0.049	0.048	0.702	0.853	0.062	0.058	0.060	0.038
Heinsberg	0.007	0.029	0.037	0.045	0.833	0.818	0.044	0.057	0.044	0.049
Kall	0.072	0.048	0.073	0.056	0.812	0.812	0.086	0.068	0.047	0.047
Selhausen	−0.031	0.038	0.051	0.043	0.780	0.888	0.064	0.056	0.056	0.041
Schönseiffen	0.015	0.017	0.036	0.038	0.908	0.868	0.045	0.048	0.043	0.045
Kleinau	0.061	0.027	0.062	0.051	0.875	0.770	0.076	0.068	0.046	0.062
Aachen	−0.113	−0.061	0.115	0.063	0.810	0.831	0.123	0.079	0.049	0.051

Table A5
Root Mean Square Error (RMSE) for Open Loop (OL), Data Assimilation With State Updates (State), Joint State-Parameter Updates (Joint), and Jackknife Simulations With Joint State-Parameter Updates (Jackknife) for the Assimilation Periods of 2016 and 2018

			RMSE (cm^3/cm^3)			
Year	Season	Mean observed soil moisture (cm^3/cm^3)	OL	State	Joint	Jackknife
2016	Spring	0.32	0.078	0.043	0.032	0.045
	Summer	0.31	0.075	0.043	0.030	0.047
	Autumn	0.25	0.070	0.039	0.030	0.048
	Winter	0.36	0.087	0.052	0.035	0.045
2018	Spring	0.31	0.076	0.046	0.037	0.062
	Summer	0.18	0.067	0.041	0.033	0.073
	Autumn	0.22	0.066	0.047	0.029	0.046
	Winter	0.33	0.065	0.042	0.031	0.043

Note. The seasonal indicator was averaged over all sites with CRNS soil moisture observations.

Table A6
Comparison of Daily Measured Evapotranspiration and Simulated Evapotranspiration From Open Loop (OL), Data Assimilation With State Updates (State), and Joint State-Parameter Updates (Joint) for Two Assimilation Periods (2016 and 2018)

Site	Year	Simulation	BIAS (mm/day)	MAE (mm/day)	R	RMSE (mm/day)	ubRMSD (mm/day)
Rollesbroich	2016	OL	−0.334	0.464	0.896	0.612	0.513
		State	−0.318	0.444	0.902	0.582	0.487
		Joint	−0.264	0.428	0.897	0.559	0.493
	2018	OL	−0.420	0.547	0.900	0.747	0.618
		State	−0.426	0.553	0.900	0.753	0.621
		Joint	−0.469	0.593	0.880	0.816	0.668
Wüstebach	2016	OL	−0.590	0.707	0.821	0.914	0.698
		State	−0.553	0.675	0.826	0.876	0.679
		Joint	−0.528	0.663	0.824	0.860	0.679
	2018	OL	−0.377	0.619	0.773	0.849	0.760
		State	−0.377	0.610	0.769	0.844	0.755
		Joint	−0.345	0.601	0.775	0.825	0.750
Selhausen	2016	OL	−0.464	0.643	0.724	0.843	0.704
		State	−0.278	0.585	0.719	0.768	0.716
		Joint	−0.239	0.568	0.723	0.753	0.714
	2018	OL	−0.268	0.629	0.710	0.871	0.829
		State	−0.183	0.612	0.713	0.842	0.822
		Joint	−0.127	0.585	0.731	0.811	0.801

CLM computes the evaporation and transpiration by taking into account both vegetated and non-vegetated surfaces (Oleson et al., 2007).

For the non-vegetated surface (bare soil), the evaporation E_g [M/L^2/T] from ground is calculated as:

$$E_g = -\frac{\rho_{\text{atm}}\left(q_{\text{atm}} - q_g\right)}{\gamma_{\text{aw}}} \quad \text{(A1)}$$

where ρ_{atm} [M/L^3] is air density, q_{atm} [M/M] is the atmospheric specific humidity, q_g [M/M] is the specific humidity of the soil surface and γ_{aw} [T/L] is the aerodynamic resistance to water vapor transfer. q_g is proportional to the saturation specific humidity:

$$q_g = \alpha q_{sat}^{T_g} \tag{A2}$$

and q_{sat}^{Tg} [M/M] is the saturated specific humidity given the ground surface temperature T_g [Q]. The factor α [−] is a combined value of soil and snow:

$$\alpha = \alpha_{soi,1}(1 - f_{sno}) + f_{sno} \tag{A3}$$

where f_{sno} [−] is the fraction of snow coverage, $\alpha_{soi,1}$ [−] refers to the surface soil layer and is a function of the surface soil layer water matrix potential ψ_1 [L]:

$$\alpha_{soi,1} = \exp\left(\frac{\psi_1 g}{1 \times 10^3 R_{wv} T_g}\right) \tag{A4}$$

where R_{wv} [L^2/T^2/Q] is the gas constant for water vapor, g [L/T^2] is the gravitational acceleration, ψ_1 [L] is calculated as:

$$\psi_1 = \psi_{sat,1} s_1^{-B_1} \text{ and } \psi_1 \geq -1 \times 10^8 \tag{A5}$$

where $\psi_{sat,1}$ [L] is saturated matric potential for the surface soil layer, B_1 [−] is the Clapp and Hornberger parameter (Clapp & Hornberger, 1978), and s_1 [−] is the wetness of the top soil layer with respect to saturation:

$$s_1 = \frac{1}{\Delta z_1 \theta_{sat,1}}\left[\frac{w_{liq,1}}{\rho_{liq}} + \frac{w_{ice,1}}{\rho_{ice}}\right] \text{ and } 0.01 \leq s_1 \leq 1.0 \tag{A6}$$

where Δz_1 [L] is the thickness of the top soil layer, $\theta_{sat,1}$ [L^3/L^3] is saturated soil moisture of the top soil layer (i.e., porosity), $w_{liq,1}$ [M/L^2] and $w_{ice,1}$ [M/L^2] are the mass of liquid water and ice of the top soil layer, ρ_{liq} [M/L^3] and ρ_{ice} [M/L^3] are the density of liquid water and ice.

For the vegetated surface, the evapotranspiration flux E [M/L^2/T] includes the water vapor flux from vegetation E_v and the ground E_g:

$$E = E_v + E_g \tag{A7}$$

$$E_v = -\frac{\rho_{atm}\left(q_s - q_{sat}^{T_v}\right)}{r_{total}} \tag{A8}$$

$$E_g = -\frac{\rho_{atm}\left(q_s - q_g\right)}{r'_{aw}} \tag{A9}$$

where q_{sat}^{Tg} [M/M] is the saturated specific humidity given the vegetation temperature T_v [Q], r' aw [T/L] is the aerodynamic resistance to water vapor transfer between the ground and the canopy air, r_{total} [T/L] is the aerodynamic resistance to water vapor transfer from the canopy to the canopy air. q_s [M/M] is the canopy specific humidity:

$$q_s = \frac{c_a^w q_{atm} + c_g^w q_g + c_v^w q_{sat}^{T_v}}{c_a^w + c_g^w + c_v^w} \tag{A10}$$

where C_a^w [L/T], C_g^w [L/T] and C_v^w [L/T] are water vapor conductances from the canopy air to the atmosphere, the leaf to canopy air, and ground to canopy air, respectively.

10.1029/2023WR035056

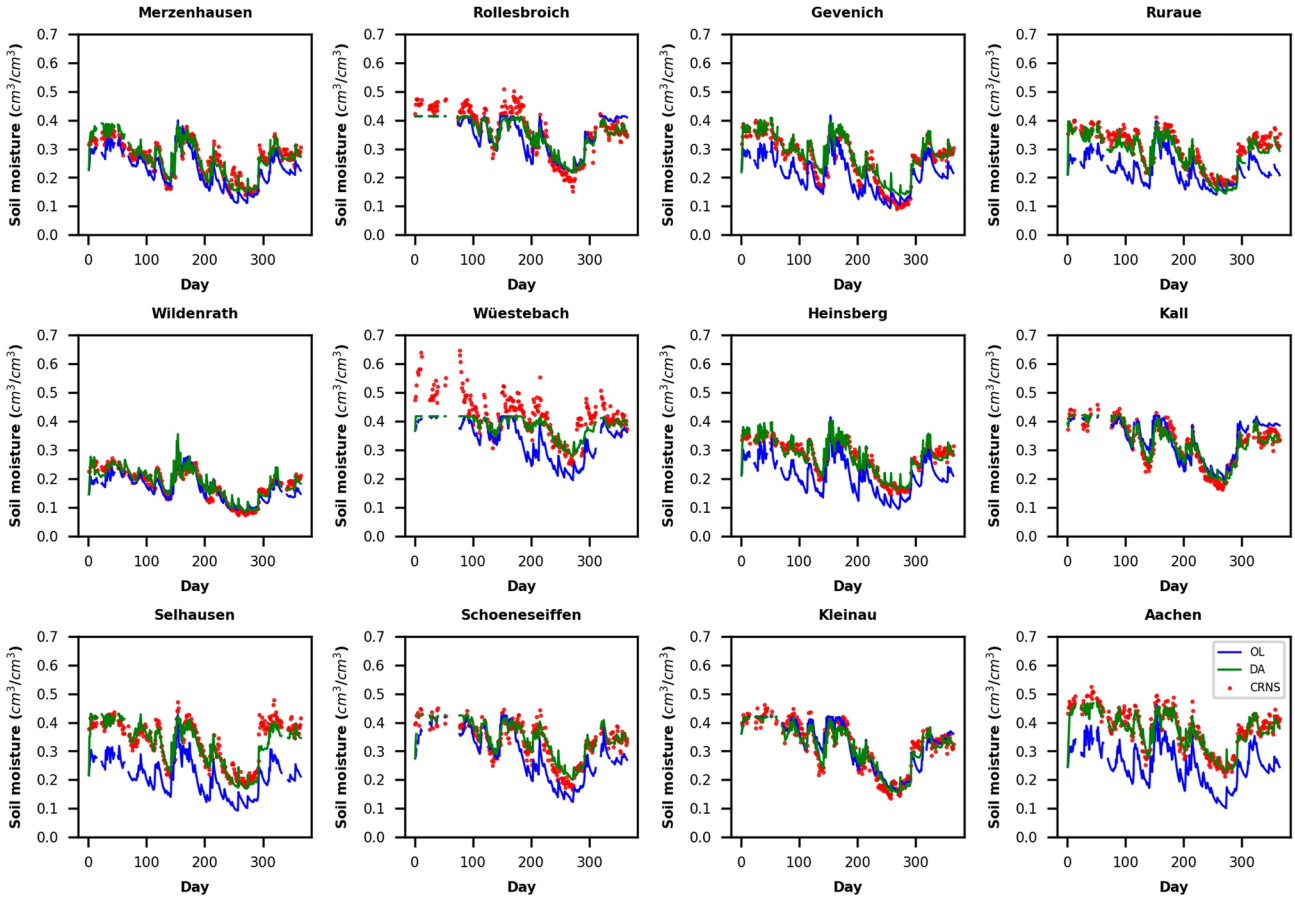

Figure A1. Temporal evolution of mean simulated soil moisture from the open loop (OL, blue), joint state-parameter estimation (DA, green), together with observed soil moisture from CRNS (red), for the year 2016 at the CRNS sites. Simulated soil moisture was vertically weighted using the revised method.

10.1029/2023WR035056

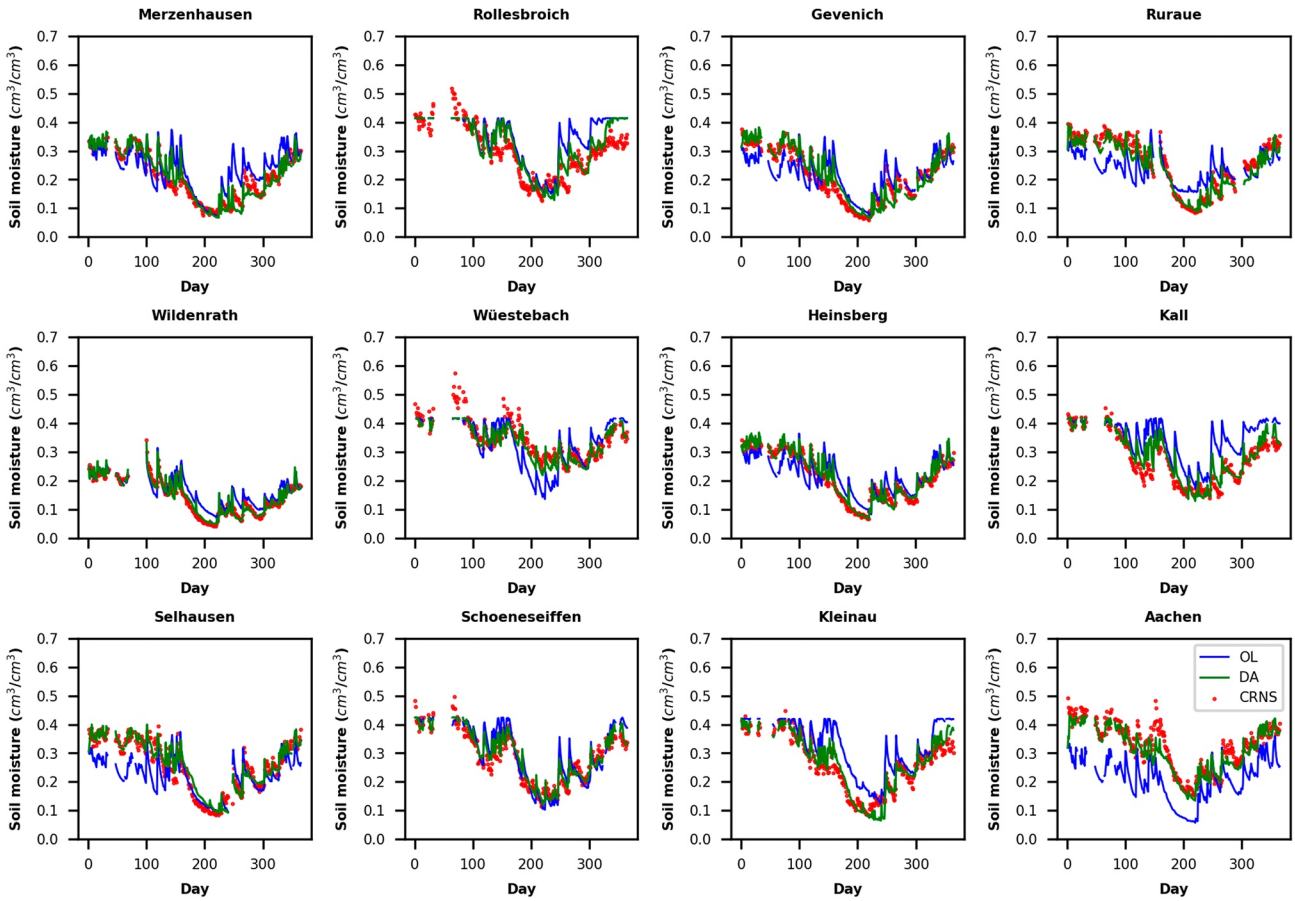

Figure A2. Temporal evolution of mean simulated soil moisture from the open loop (OL, blue), joint state-parameter estimation (DA, green), together with observed soil moisture from CRNS (red), for the year 2018 at the CRNS sites. Simulated soil moisture was vertically weighted using the revised method.

10.1029/2023WR035056

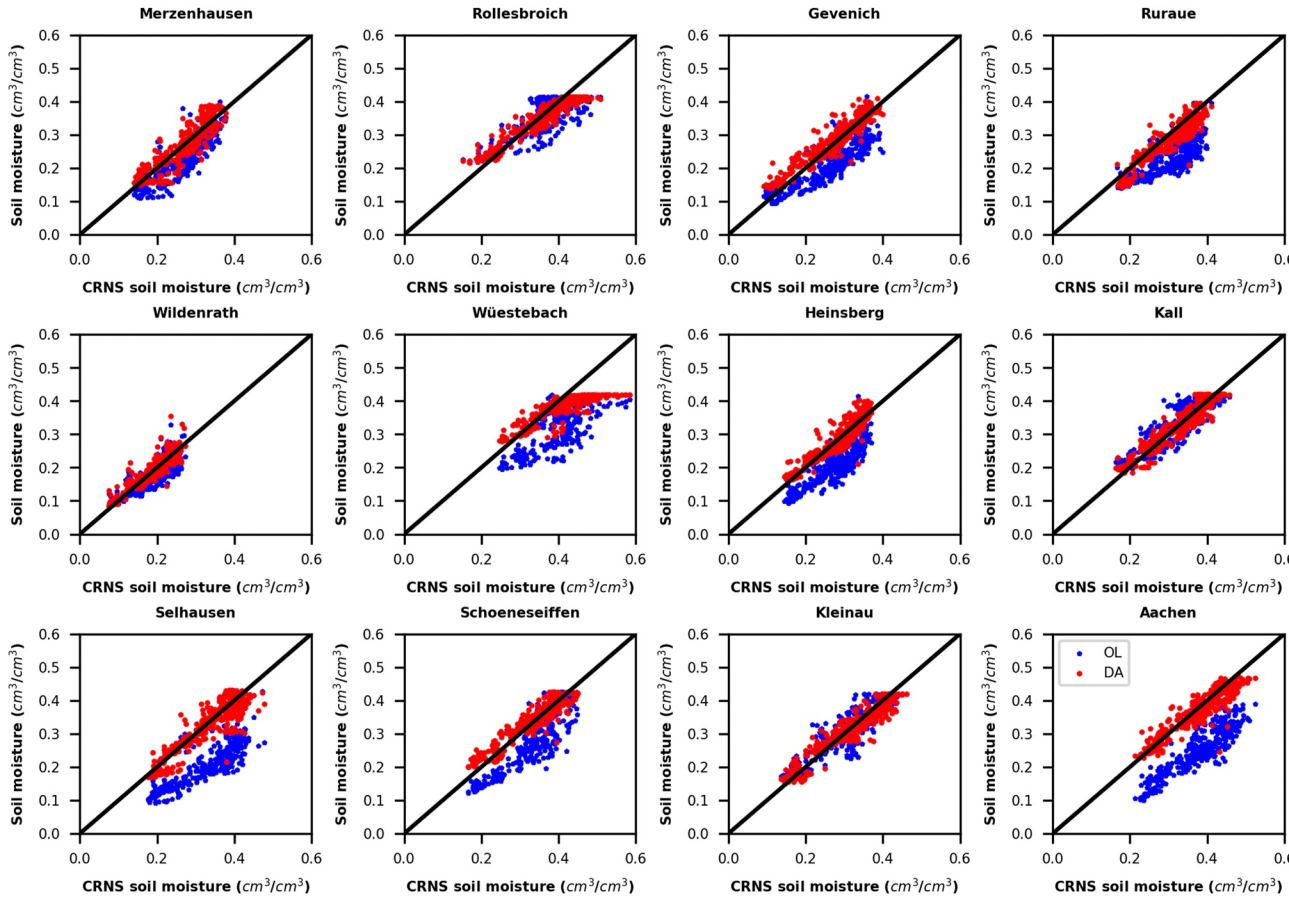

Figure A3. Soil moisture scatter plots for CRNS observations versus ensemble mean soil moisture from the open loop run (OL, blue) and ensemble mean soil moisture from joint state-parameter estimation (DA, red) for 2016.

10.1029/2023WR035056

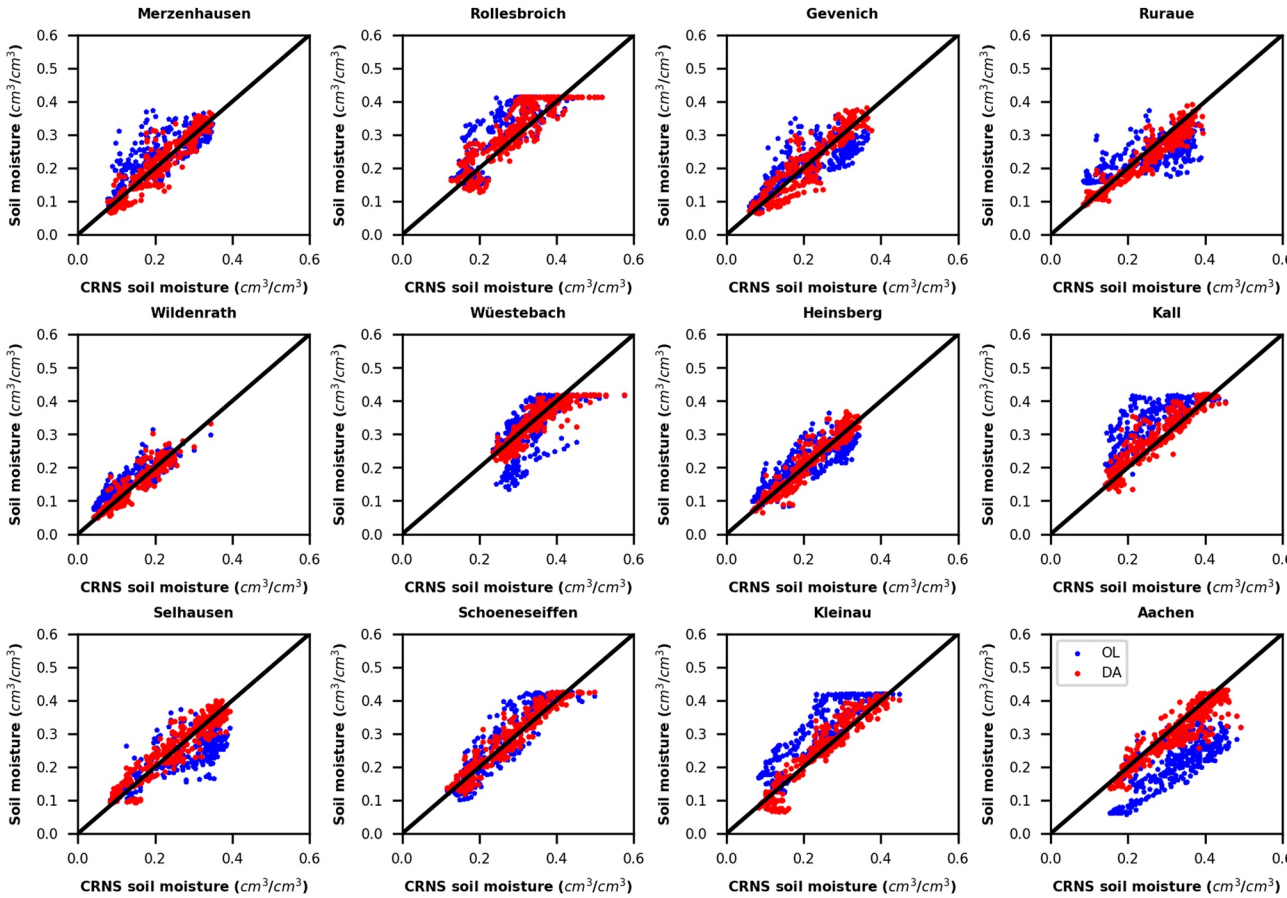

Figure A4. Soil moisture scatter plots for CRNS observations versus ensemble mean soil moisture from the open loop run (OL, blue) and ensemble mean soil moisture from joint state-parameter estimation (DA, red) for 2018.

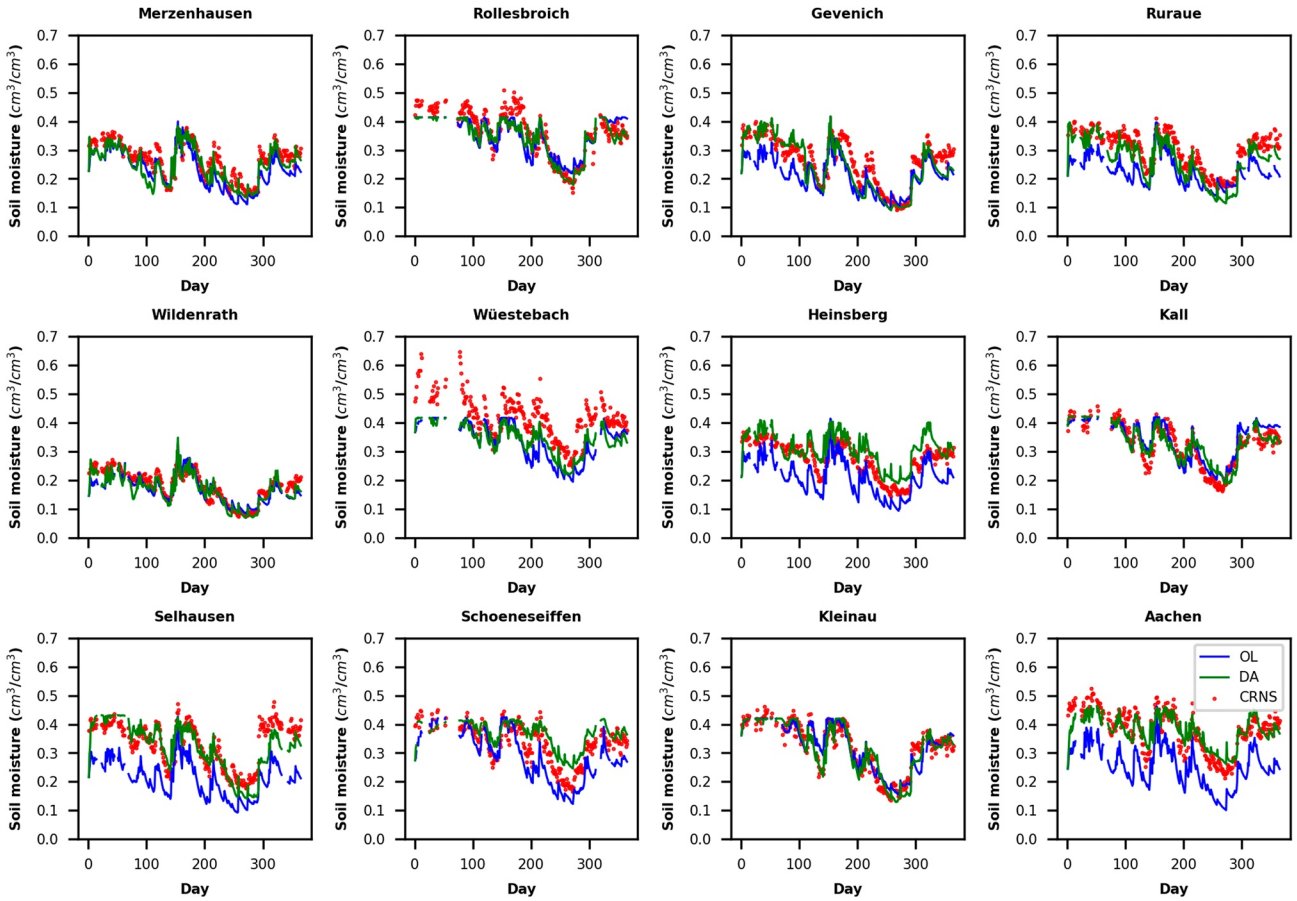

Figure A5. Temporal evolution of mean simulated soil moisture from the open loop run (OL, blue), jackknife simulations (DA, green), together with the observed soil moisture from CRNS (red) for the year 2016 at the CRNS sites. Simulated soil moisture was vertically weighted using the revised method.

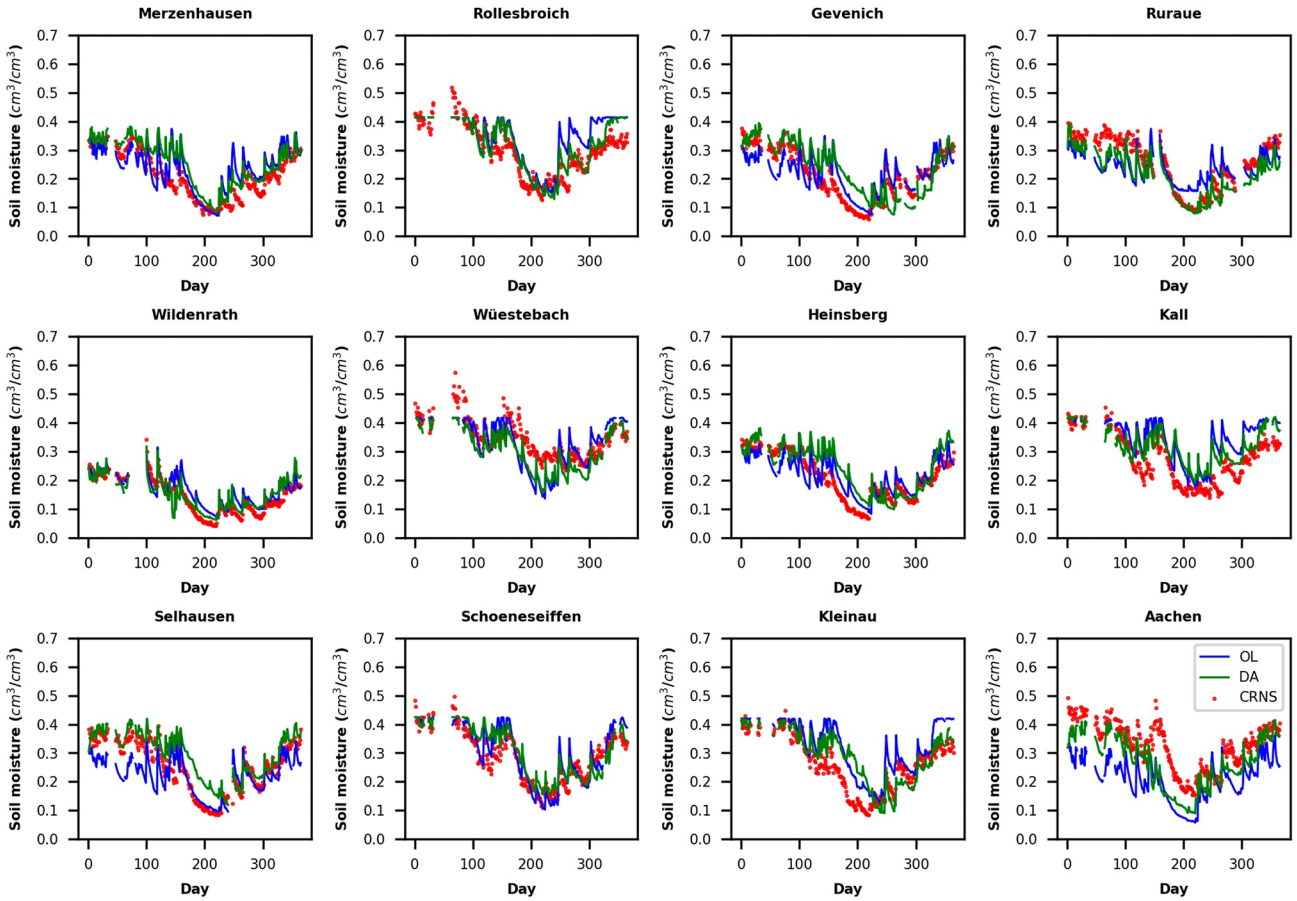

Figure A6. Temporal evolution of mean simulated soil moisture from the open loop run (OL, blue), jackknife simulations (DA, green), together with the observed soil moisture from CRNS (red) for the year 2018 at the CRNS sites. Simulated soil moisture was vertically weighted using the revised method.

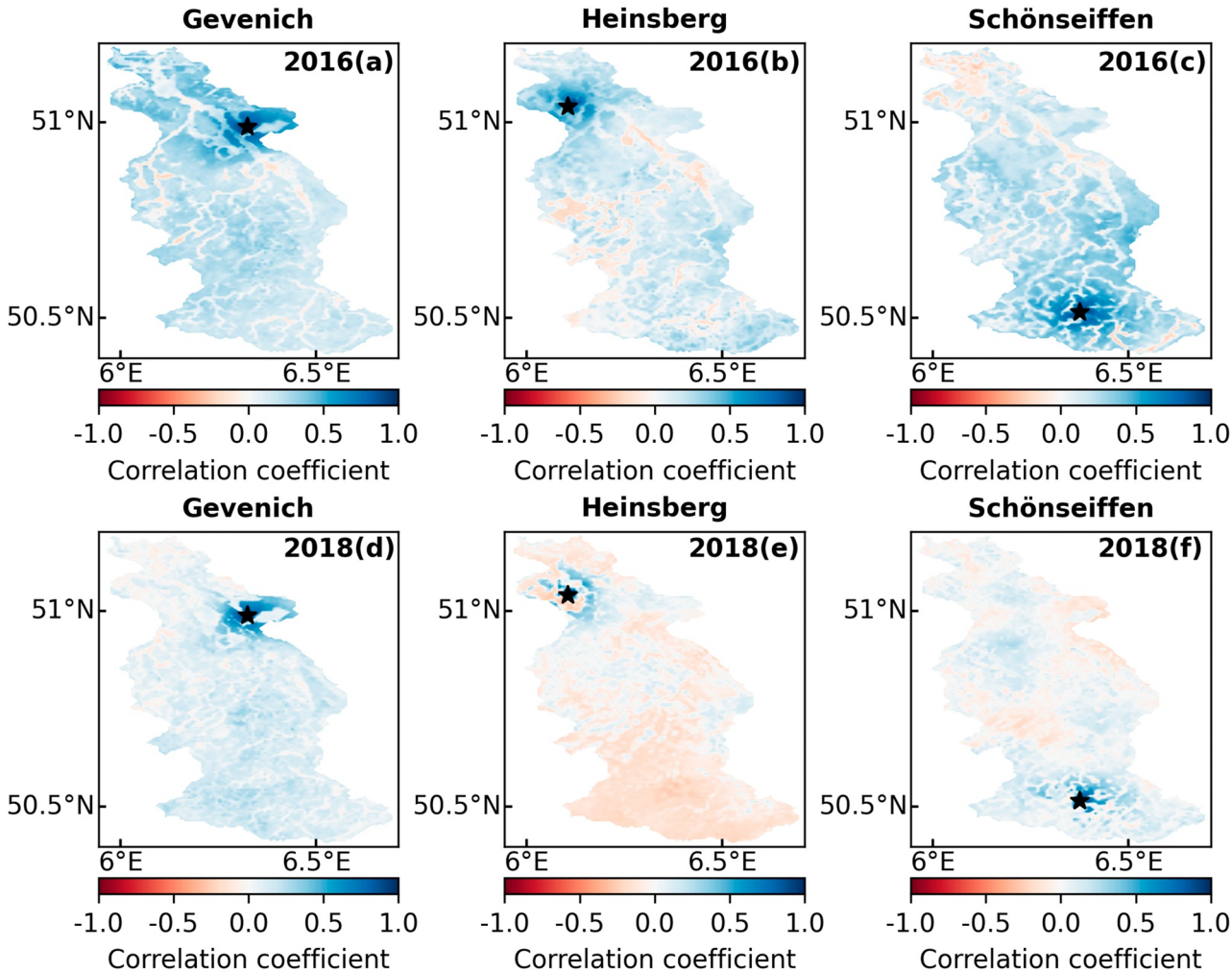

Figure A7. Examples of the spatial correlations of soil moisture between CRNS sites and other grid cells over the Rur catchment, for the open loop run. Subplots (a) and (d) are from Gevenich on the 29th of June in 2016 and 2018, (b) and (e) are from Heinsberg on the second of August in 2016 and 2018, and (c) and (f) are from Schönseiffen on the 28th of July in 2016 and 2018. The black asterisk is the location of the CRNS sites.

Data Availability Statement

The atmospheric reanalysis data set COSMO-REA6 (Bollmeyer et al., 2015; Wahl et al., 2017) was downloaded from (https://reanalysis.meteo.uni-bonn.de/?COSMO-REA6; last access: 17 August 2023). The soil map BK50 (Geologischer Dienst Nordrhein-Westfalen, 2009) was downloaded from (https://www.opengeodata.nrw.de/produkte/geologie/boden/BK/ISBK50/; last access: 17 August 2023), and the European Soil Database (ESDB) (Pano, 2006) was available at (https://esdac.jrc.ec.europa.eu/content/european-soil-database-v20-vector-and-attribute-data; last access: 17 August 2023). The aquifer permeability map can be found at (https://www.opengeodata.nrw.de/produkte/geologie/geologie/HK/ISHK100/; last access: 17 August 2023), processed to 100 m by Herrmann et al. (2015). The eddy covariance and discharge data were obtained from TERENO at (https://www.tereno.net/; last access: 17 August 2023). The CRNS soil moisture data were retrieved from the "Data set of COSMOS-Europe: A European network of Cosmic-Ray Neutron Soil Moisture Sensors" (Bogena et al., 2022), at [https://doi.org/10.34731/x9s3-kr48; last access: 17 August 2023]). The remote repository of TSMP is located on Github at (https://github.com/HPSCTerrSys/TSMP; last access: 17 August 2023). PDAF version 1.13.2 can be downloaded at (http://pdaf.awi.de/trac/wiki; last access: 17 August 2023) after registration. Figures were made with Matplotlib version 3.5.2 (Hunter, 2007), available under the Matplotlib license at (https://matplotlib.org/; last access: 17 August 2023).

Acknowledgments
This work was funded by the China Scholarship Council (CSC), Grant: 201904910448. HJHF gratefully acknowledges the support provided by the project DETECT: Funded by the Deutsche Forschungsgemeinschaft (DFG, German Research Foundation)-SFB 1502/1-2022-Project number: 450058266. Furthermore, the authors gratefully acknowledge the computing time granted by the supercomputer JUWELS at Forschungszentrum Jülich. We would also like to thank the Terrestrial Environmental Observatories (TERENO) network, funded by the Helmholtz Association. Finally, the authors would like to thank three anonymous reviewers for their constructive comments and suggestions to improve the quality of our paper. Open Access funding enabled and organized by Projekt DEAL.

References

Allan, R., Pereira, L., & Smith, M. (1998). Crop evapotranspiration-Guidelines for computing crop water requirements-FAO irrigation and drainage (p. 56).

Andreasen, M., Jensen, K. H., Desilets, D., Franz, T. E., Zreda, M., Bogena, H. R., & Looms, M. C. (2017). Status and perspectives on the cosmic-ray neutron method for soil moisture estimation and other environmental science applications. *Vadose Zone Journal*, *16*(8), 1–11. https://doi.org/10.2136/vzj2017.04.0086

Ashby, S. F., & Falgout, R. D. (1996). A parallel multigrid preconditioned conjugate gradient algorithm for groundwater flow simulations. *Nuclear Science and Engineering*, *124*(1), 145–159. https://doi.org/10.13182/nse96-a24230

Baatz, D., Kurtz, W., Hendricks Franssen, H. J., Vereecken, H., & Kollet, S. J. (2017). Catchment tomography—An approach for spatial parameter estimation. *Advances in Water Resources*, *107*, 147–159. https://doi.org/10.1016/j.advwatres.2017.06.006

Baatz, R., Hendricks Franssen, H.-J., Han, X., Hoar, T., Bogena, H. R., & Vereecken, H. (2017). Evaluation of a cosmic-ray neutron sensor network for improved land surface model prediction. *Hydrology and Earth System Sciences*, *21*(5), 2509–2530. https://doi.org/10.5194/hess-21-2509-2017

Baldauf, M., Seifert, A., Förstner, J., Majewski, D., Raschendorfer, M., & Reinhardt, T. (2011). Operational convective-scale numerical weather prediction with the COSMO model: Description and sensitivities. *Monthly Weather Review*, *139*(12), 3887–3905. https://doi.org/10.1175/mwr-d-10-05013.1

Baroni, G., Zink, M., Kumar, R., Samaniego, L., & Attinger, S. (2017). Effects of uncertainty in soil properties on simulated hydrological states and fluxes at different spatio-temporal scales. *Hydrology and Earth System Sciences*, *21*(5), 2301–2320. https://doi.org/10.5194/hess-21-2301-2017

Bauer-Marschallinger, B., Freeman, V., Cao, S., Paulik, C., Schaufler, S., Stachl, T., et al. (2019). Toward global soil moisture monitoring with Sentinel-1: Harnessing assets and overcoming obstacles. *IEEE Transactions on Geoscience and Remote Sensing*, *57*(1), 520–539. https://doi.org/10.1109/TGRS.2018.2858004

Boas, T., Bogena, H., Grünwald, T., Heinesch, B., Ryu, D., Schmidt, M., et al. (2021). Improving the representation of cropland sites in the Community Land Model (CLM) version 5.0. *Geoscientific Model Development*, *14*(1), 573–601. https://doi.org/10.5194/gmd-14-573-2021

Bogena, H. R., Herbst, M., Hake, J. F., Kunkel, R., Montzka, C. P. T., Vereecken, H., & Wendland, F. (2005). *MOSYRUR: Water balance analysis in the Rur basin*. Forschungszentrum Jülich.

Bogena, H. R., Herrmann, F., Jakobi, J., Brogi, C., Ilias, A., Huisman, J. A., et al. (2020). Monitoring of snowpack dynamics with cosmic-ray neutron probes: A comparison of four conversion methods. *Frontiers in Water*, *2*. https://doi.org/10.3389/frwa.2020.00019

Bogena, H. R., Huisman, J. A., Güntner, A., Hübner, C., Kusche, J., Jonard, F., et al. (2015). *Emerging methods for noninvasive sensing of soil moisture dynamics from field to catchment scale: A review* (Vol. 2, pp. 635–647). Wiley Interdisciplinary Reviews-Water. https://doi.org/10.1002/wat2.1097

Bogena, H. R., Montzka, C., Huisman, J. A., Graf, A., Schmidt, M., Stockinger, M., et al. (2018). The TERENO-Rur hydrological observatory: A multiscale multi-compartment Research platform for the advancement of hydrological science. *Vadose Zone Journal*, *17*(1), 1–22. https://doi.org/10.2136/vzj2018.03.0055

Bogena, H. R., Schrön, M., Jakobi, J., Ney, P., Zacharias, S., Andreasen, M., et al. (2022). COSMOS-Europe: A European network of cosmic-ray neutron soil moisture sensors. *Earth System Science Data*, *14*(3), 1125–1151. https://doi.org/10.5194/essd-14-1125-2022

Bollmeyer, C., Keller, J. D., Ohlwein, C., Wahl, S., Crewell, S., Friederichs, P., et al. (2015). Towards a high-resolution regional reanalysis for the European CORDEX domain. *Quarterly Journal of the Royal Meteorological Society*, *141*(686), 1–15. https://doi.org/10.1002/qj.2486

Bonan, G. B., Levis, S., Kergoat, L., & Oleson, K. W. (2002). Landscapes as patches of plant functional types: An integrating concept for climate and ecosystem models. *Global Biogeochemical Cycles*, *16*(2), 5-1–5-23. https://doi.org/10.1029/2000GB001360

Brandhorst, N., & Neuweiler, I. (2023). Impact of parameter updates on soil moisture assimilation in a 3D heterogeneous hillslope model. *Hydrology and Earth System Sciences*, *27*(6), 1301–1323. https://doi.org/10.5194/hess-27-1301-2023

Camporese, M., Paniconi, C., Putti, M., & Salandin, P. (2009). Ensemble Kalman filter data assimilation for a process-based catchment scale model of surface and subsurface flow. *Water Resources Research*, *45*(10), 1–14. https://doi.org/10.1029/2008wr007031

Chen, X., & Hu, Q. (2004). Groundwater influences on soil moisture and surface evaporation. *Journal of Hydrology*, *297*(1–4), 285–300. https://doi.org/10.1016/j.jhydrol.2004.04.019

Clapp, R. B., & Hornberger, G. M. (1978). Empirical equations for some soil hydraulic properties. *Water Resources Research*, *14*(4), 601–604. https://doi.org/10.1029/wr014i004p00601

De Lannoy, G. J. M., Reichle, R. H., & Vrugt, J. A. (2014). Uncertainty quantification of GEOS-5 L-band radiative transfer model parameters using Bayesian inference and SMOS observations. *Remote Sensing of Environment*, *148*, 146–157. https://doi.org/10.1016/j.rse.2014.03.030

Evensen, G. (1994). Sequential data assimilation with a nonlinear quasi-geostrophic model using Monte Carlo methods to forecast error statistics. *Journal of Geophysical Research*, *99*(C5), 10143–110162. https://doi.org/10.1029/94jc00572

Evensen, G. (2003). The ensemble Kalman filter: Theoretical formulation and practical implementation. *Ocean Dynamics*, *53*(4), 343–367. https://doi.org/10.1007/s10236-003-0036-9

Fersch, B., Francke, T., Heistermann, M., Schrön, M., Döpper, V., Jakobi, J., et al. (2020). A dense network of cosmic-ray neutron sensors for soil moisture observation in a highly instrumented pre-Alpine headwater catchment in Germany. *Earth System Science Data*, *12*(3), 2289–2309. https://doi.org/10.5194/essd-12-2289-2020

Finkele, K., Hochstrasser, T., Murphy, P. N. C., Daly, E., Jarmain, C., Richards, K., et al. (2022). *The new Irish soil moisture observation network—ISMON: An umbrella for integrating several recent soil moisture measurements initiatives* (pp. EMS2022). EMS Annual Meeting 2022. https://doi.org/10.5194/ems2022-273

Franz, T. E., Zreda, M., Ferre, T. P. A., Rosolem, R., Zweck, C., Stillman, S., et al. (2012). Measurement depth of the cosmic ray soil moisture probe affected by hydrogen from various sources. *Water Resources Research*, *48*(8), W08515. https://doi.org/10.1029/2012WR011871

Freeze, R. A. (1975). A stochastic-conceptual analysis of the one-dimensional groundwater flow in nonuniform homogeneous media. *Water Resources Research*, *11*(15), 725–742. https://doi.org/10.1029/WR011i005p00725

Furusho-Percot, C., Goergen, K., Hartick, C., Kulkarni, K., Keune, J., & Kollet, S. (2019). Pan-European groundwater to atmosphere terrestrial systems climatology from a physically consistent simulation. *Scientific Data*, *6*, 1–9. https://doi.org/10.1038/s41597-019-0328-7

Gebler, S., Kurtz, W., Pauwels, V. R. N., Kollet, S. J., Vereecken, H., & Hendricks Franssen, H. J. (2019). Assimilation of high-resolution soil moisture data into an integrated terrestrial model for a small-scale head-water catchment. *Water Resources Research*, *55*(12), 10358–10385. https://doi.org/10.1029/2018wr024658

Geologischer Dienst Nordrhein-Westfalen. (2009). Geologischer Dienst Nordrhein-Westfalen informationssystem Bodenkarte 1: 50 000 [Dataset]. Retrieved from https://www.opengeodata.nrw.de/produkte/geologie/boden/BK/ISBK50/

Han, X., Franssen, H. J. H., Rosolem, R., Jin, R., Li, X., & Vereecken, H. (2015). Correction of systematic model forcing bias of CLM using assimilation of cosmic-ray neutrons and land surface temperature: A study in the heihe catchment, China. *Hydrology and Earth System Sciences*, *19*(1), 615–629. https://doi.org/10.5194/hess-19-615-2015

Han, X., Hendricks Franssen, H.-J., Jiménez Bello, M. Á., Rosolem, R., Bogena, H., Alzamora, F. M., et al. (2016). Simultaneous soil moisture and properties estimation for a drip irrigated field by assimilating cosmic-ray neutron intensity. *Journal of Hydrology*, *539*, 611–624. https://doi.org/10.1016/j.jhydrol.2016.05.050

Han, X., Hendricks Franssen, H.-J., Li, X., Zhang, Y., Montzka, C., & Vereecken, H. (2013). Joint assimilation of surface temperature and L-band microwave brightness temperature in land data assimilation. *Vadose Zone Journal*, *12*(3), vzj2012.0072. https://doi.org/10.2136/vzj2012.0072

He, H., Aogu, K., Li, M., Xu, J., Sheng, W., Jones, S. B., et al. (2021). Chapter Three—A review of time domain reflectometry (TDR) applications in porous media. In D. L. Sparks (Ed.), *Advances in agronomy* (pp. 83–155). Academic Press. https://doi.org/10.1016/bs.agron.2021.02.003

Heistermann, M., Bogena, H., Francke, T., Güntner, A., Jakobi, J., Rasche, D., et al. (2022). Soil moisture observation in a forested headwater catchment: Combining a dense cosmic-ray neutron sensor network with roving and hydrogravimetry at the TERENO site Wüstebach. *Earth System Science Data*, *14*(5), 2501–2519. https://doi.org/10.5194/essd-14-2501-2022

Hendricks Franssen, H. J., & Kinzelbach, W. (2008). Real-time groundwater flow modeling with the Ensemble Kalman Filter: Joint estimation of states and parameters and the filter inbreeding problem. *Water Resources Research*, *44*(9), 1–22. https://doi.org/10.1029/2007wr006505

Herrmann, F., Keller, L., Kunkel, R., Vereecken, H., & Wendland, F. (2015). Determination of spatially differentiated water balance components including groundwater recharge on the Federal State level—A case study using the mGROWA model in North Rhine-Westphalia (Germany). *Journal of Hydrology: Regional Studies*, *4*, 294–312. https://doi.org/10.1016/j.ejrh.2015.06.018

Hung, C. P., Schalge, B., Baroni, G., Vereecken, H., & Hendricks Franssen, H. J. (2022). Assimilation of groundwater level and soil moisture data in an integrated land surface-subsurface model for southwestern Germany. *Water Resources Research*, *58*(6), e2021WR031549. https://doi.org/10.1029/2021WR031549

Hunter, J. D. (2007). Matplotlib: A 2D graphics environment. *Computing in Science and Engineering*, *9*(3), 90–95. https://doi.org/10.1109/mcse.2007.55

Jarvis, A., Reuter, H. I., Nelson, A., & Guevara, E. (2008). Hole-filled SRTM for the globe: Version 4: Data grid, 2008 [Dataset]. Web publication/site, CGIAR Consortium for Spatial Information. http://srtm.csi.cgiar.org/

Jones, J. E., & Woodward, C. S. (2001). Newton–Krylov-multigrid solvers for large-scale, highly heterogeneous, variably saturated flow problems. *Advances in Water Resources*, *24*(27), 763–774. https://doi.org/10.1016/S0309-1708(00)00075-0

Keune, J., Gasper, F., Goergen, K., Hense, A., Shrestha, P., Sulis, M., & Kollet, S. (2016). Studying the influence of groundwater representations on land surface-atmosphere feedbacks during the European heat wave in 2003. *Journal of Geophysical Research: Atmospheres*, *121*(22), 13301–313325. https://doi.org/10.1002/2016jd025426

Kim, H., Wigneron, J.-P., Kumar, S., Dong, J., Wagner, W., Cosh, M. H., et al. (2020). Global scale error assessments of soil moisture estimates from microwave-based active and passive satellites and land surface models over forest and mixed irrigated/dryland agriculture regions. *Remote Sensing of Environment*, *251*, 112052. https://doi.org/10.1016/j.rse.2020.112052

Köhli, M., Schrön, M., Zreda, M., Schmidt, U., Dietrich, P., & Zacharias, S. (2015). Footprint characteristics revised for field-scale soilmoisture monitoring with cosmic-ray neutrons. *Water Resources Research*, *10*, 1002. https://doi.org/10.1002/2015WR017169

Kollet, S. J., & Maxwell, R. M. (2006). Integrated surface–groundwater flow modeling: A free-surface overland flow boundary condition in a parallel groundwater flow model. *Advances in Water Resources*, *29*(7), 945–958. https://doi.org/10.1016/j.advwatres.2005.08.006

Kollet, S. J., & Maxwell, R. M. (2008). Capturing the influence of groundwater dynamics on land surface processes using an integrated, distributed watershed model. *Water Resources Research*, *44*(2), 1–18. https://doi.org/10.1029/2007wr006004

Kurtz, W., He, G., Kollet, S. J., Maxwell, R. M., Vereecken, H., & Hendricks Franssen, H.-J. (2016). TerrSysMP–PDAF (version 1.0): A modular high-performance data assimilation framework for an integrated land surface–subsurface model. *Geoscientific Model Development*, *9*(4), 1341–1360. https://doi.org/10.5194/gmd-9-1341-2016

Li, D., Schrön, M., Köhli, M., Bogena, H., Weimar, J., Jiménez Bello, M. A., et al. (2019). Can drip irrigation be scheduled with cosmic-ray neutron sensing? *Vadose Zone Journal*, *18*(1), 190053. https://doi.org/10.2136/vzj2019.05.0053

Li, S., Zhang, L., Ma, R., Yan, M., & Tian, X. (2020). Improved ET assimilation through incorporating SMAP soil moisture observations using a coupled process model: A study of U.S. Arid and semiarid regions. *Journal of Hydrology*, *590*, 125402. https://doi.org/10.1016/j.jhydrol.2020.125402

Lighthill, M. J., & Whitham, G. B. (1955). On kinematic waves I. Flood movement in long rivers. *Proceedings of the Royal Society of London. Series A. Mathematical, Physical and Engineering Sciences*, *229*, 281–316. https://doi.org/10.1098/rspa.1955.0088

Mauder, M., Cuntz, M., Drüe, C., Graf, A., Rebmann, C., Schmid, H. P., et al. (2013). A strategy for quality and uncertainty assessment of long-term eddy-covariance measurements. *Agricultural and Forest Meteorology*, *169*, 122–135. https://doi.org/10.1016/j.agrformet.2012.09.006

Maxwell, R. M. (2013). A terrain-following grid transform and preconditioner for parallel, large-scale, integrated hydrologic modeling. *Advances in Water Resources*, *53*, 109–117. https://doi.org/10.1016/j.advwatres.2012.10.001

McLaughlin, D. (2002). An integrated approach to hydrologic data assimilation: Interpolation, smoothing, and filtering. *Advances in Water Resources*, *25*(8–12), 1275–1286. https://doi.org/10.1016/S0309-1708(02)00055-6

Montzka, C., Canty, M., Kunkel, R., Menz, G., Vereecken, H., & Wendland, F. (2008). Modelling the water balance of a mesoscale catchment basin using remotely sensed land cover data. *Journal of Hydrology*, *353*(3–4), 322–334. https://doi.org/10.1016/j.jhydrol.2008.02.018

Oleson, K., Dai, Y., Bonan, G. B., Bosilovichm, M., Dickinson, R., Dirmeyer, P., & Zeng, X. (2004). *Technical description of the community land model (CLM)* (pp. 1–187). University Corporation for Atmospheric Research. https://doi.org/10.5065/D6N877R0

Oleson, K. W., Niu, G.-Y., Yang, Z.-L., Lawrence, D. M., Thornton, P. E., Lawrence, P. J., et al. (2007). CLM3.5 documentation.

Oleson, K. W., Niu, G. Y., Yang, Z. L., Lawrence, D. M., Thornton, P. E., Lawrence, P. J., et al. (2008). Improvements to the Community Land Model and their impact on the hydrological cycle. *Journal of Geophysical Research*, *113*(G1), 1–26. https://doi.org/10.1029/2007jg000563

Pano, P. (2006). The European soil database GEO: Connexion [Dataset]. *5*(7), 32–33. https://esdac.jrc.ec.europa.eu/content/european-soil-database-v20-vector-and-attribute-data

Patil, A., Fersch, B., Hendricks Franssen, H.-J., & Kunstmann, H. (2021). Assimilation of cosmogenic neutron counts for improved soil moisture prediction in a distributed land surface model. *Frontiers in Water*, *3*. https://doi.org/10.3389/frwa.2021.729592

Reichle, R. H., Kumar, S. V., Mahanama, S. P. P., Koster, R. D., & Liu, Q. (2010). Assimilation of satellite-derived skin temperature observations into land surface models. *Journal of Hydrometeorology*, *11*(5), 1103–1122. https://doi.org/10.1175/2010JHM1262.1

Richards, L. (1931). Capillary conduction of liquids through porous mediums. *Journal of Applied Physics*, *1*(5), 318–333. https://doi.org/10.1063/1.1745010

Ridler, M.-E., Madsen, H., Stisen, S., Bircher, S., & Fensholt, R. (2014). Assimilation of SMOS-derived soil moisture in a fully integrated hydrological and soil-vegetation-atmosphere transfer model in Western Denmark. *Water Resources Research*, *50*(11), 8962–8981. https://doi.org/10.1002/2014WR015392

Rosolem, R., Hoar, T., Arellano, A., Anderson, J. L., Shuttleworth, W. J., Zeng, X., & Franz, T. E. (2014). Translating aboveground cosmic-ray neutron intensity to high-frequency soil moisture profiles at sub-kilometer scale. *Hydrology and Earth System Sciences*, *18*(11), 4363–4379. https://doi.org/10.5194/hess-18-4363-2014

Schaap, M. G., Leij, F. J., & van Genuchten, M. T. (2001). Rosetta: A computer program for estimating soil hydraulic parameters with hierarchical pedotransfer functions. *Journal of Hydrology*, *251*(3–4), 163–176. https://doi.org/10.1016/S0022-1694(01)00466-8

Schöniger, A., Nowak, W., & Hendricks Franssen, H.-J. (2012). Parameter estimation by ensemble Kalman filters with transformed data: Approach and application to hydraulic tomography. *Water Resources Research*, *48*(4), W04502. https://doi.org/10.1029/2011WR010462

Schrön, M., Köhli, M., Scheiffele, L., Iwema, J., Bogena, H. R., Lv, L., et al. (2017). Improving calibration and validation of cosmic-ray neutron sensors in the light of spatial sensitivity. *Hydrology and Earth System Sciences*, *21*(10), 5009–5030. https://doi.org/10.5194/hess-21-5009-2017

Shrestha, P., Kurtz, W., Vogel, G., Schulz, J. P., Sulis, M., Hendricks Franssen, H. J., et al. (2018). Connection between root zone soil moisture and surface energy flux partitioning using modeling, observations, and data assimilation for a temperate grassland site in Germany. *Journal of Geophysical Research: Biogeosciences*, *123*(9), 2839–2862. https://doi.org/10.1029/2016JG003753

Shrestha, P., Sulis, M., Masbou, M., Kollet, S., & Simmer, C. (2014). A scale-consistent terrestrial systems modeling platform based on COSMO, CLM, and ParFlow. *Monthly Weather Review*, *142*(9), 3466–3483. https://doi.org/10.1175/mwr-d-14-00029.1

Shrestha, P., Sulis, M., Simmer, C., & Kollet, S. (2015). Impacts of grid resolution on surface energy fluxes simulated with an integrated surface-groundwater flow model. *Hydrology and Earth System Sciences*, *19*(10), 4317–4326. https://doi.org/10.5194/hess-19-4317-2015

Shrestha, P., Sulis, M., Simmer, C., & Kollet, S. (2018). Effects of horizontal grid resolution on evapotranspiration partitioning using TerrSysMP. *Journal of Hydrology*, *557*, 910–915. https://doi.org/10.1016/j.jhydrol.2018.01.024

Shuttleworth, J., Rosolem, R., Zreda, M., & Franz, T. (2013). The COsmic-ray soil moisture interaction Code (COSMIC) for use in data assimilation. *Hydrology and Earth System Sciences*, *17*(8), 3205–3217. https://doi.org/10.5194/hess-17-3205-2013

Strebel, L., Bogena, H. R., Vereecken, H., & Hendricks Franssen, H.-J. (2022). Coupling the community land model version 5.0 to the parallel data assimilation framework PDAF: Description and applications. *Geoscientific Model Development*, *15*(2), 395–411. https://doi.org/10.5194/gmd-15-395-2022

Sulis, M., Keune, J., Shrestha, P., Simmer, C., & Kollet, S. J. (2018). Quantifying the impact of subsurface-land surface physical processes on the predictive skill of subseasonal mesoscale atmospheric simulations. *Journal of Geophysical Research: Atmospheres*, *123*(17), 9131–9151. https://doi.org/10.1029/2017JD028187

Sulis, M., Langensiepen, M., Shrestha, P., Schickling, A., Simmer, C., & Kollet, S. J. (2015). Evaluating the influence of plant-specific physiological parameterizations on the partitioning of land surface energy fluxes. *Journal of Hydrometeorology*, *16*(2), 517–533. https://doi.org/10.1175/jhm-d-14-0153.1

Turner, M., Walker, J., & Oke, P. (2008). Ensemble member generation for sequential data assimilation. *Remote Sensing of Environment*, *112*(4), 1421–1433. https://doi.org/10.1016/j.rse.2007.02.042

Valcke, S. (2013). The OASIS3 coupler: A European climate modelling community software. *Geoscientific Model Development*, *6*(2), 373–388. https://doi.org/10.5194/gmd-6-373-2013

Vereecken, H., Amelung, W., Bauke, S. L., Bogena, H., Brüggemann, N., Montzka, C., et al. (2022). Soil hydrology in the Earth system. *Nature Reviews Earth and Environment*, *3*(9), 573–587. https://doi.org/10.1038/s43017-022-00324-6

Wahl, S., Bollmeyer, C., Crewell, S., Figura, C., Friederichs, P., Hense, A., et al. (2017). A novel convective-scale regional reanalysis COSMO-REA2: Improving the representation of precipitation. *Meteorologische Zeitschrift*, *26*(4), 345–361. https://doi.org/10.1127/metz/2017/0824

Waldhoff, G., & Lussem, U. (2015). Preliminary land use classification of 2015 for the Rur catchment [Dataset]. TR32DB. https://doi.org/10.5880/TR32DB.14

Yamamoto, J. K. (2007). On unbiased backtransform of lognormal kriging estimates. *Computational Geosciences*, *11*(3), 219–234. https://doi.org/10.1007/s10596-007-9046-x

Zhang, H., Kurtz, W., Kollet, S., Vereecken, H., & Franssen, H.-J. H. (2018). Comparison of different assimilation methodologies of groundwater levels to improve predictions of root zone soil moisture with an integrated terrestrial system model. *Advances in Water Resources*, *111*, 224–238. https://doi.org/10.1016/j.advwatres.2017.11.003

Zhang, Y., & Schaap, M. G. (2017). Weighted recalibration of the Rosetta pedotransfer model with improved estimates of hydraulic parameter distributions and summary statistics (Rosetta3). *Journal of Hydrology*, *547*, 39–53. https://doi.org/10.1016/j.jhydrol.2017.01.004

Zhao, H., Montzka, C., Baatz, R., Vereecken, H., & Franssen, H.-J. H. (2021). The importance of subsurface processes in land surface modeling over a temperate region: An analysis with SMAP, cosmic ray neutron sensing and triple collocation analysis. *Remote Sensing*, *13*(16), 3068. https://doi.org/10.3390/rs13163068

Zreda, M., Desilets, D., Ferré, T. P. A., & Scott, R. L. (2008). Measuring soil moisture content non-invasively at intermediate spatial scale using cosmic-ray neutrons. *Geophysical Research Letters*, *35*(21), L2140. https://doi.org/10.1029/2008GL035655